Monthly Notices of the ROYAL ASTRONOMICAL SOCIETY

MNRAS **548,** 1–27 (2026)
Advance Access publication 2026 April 14

https://doi.org/10.1093/mnras/stag632

The Dark Energy Survey supernova program: a reanalysis of cosmology results and evidence for evolving dark energy with an updated Type Ia supernova calibration

B. Popovic [1,2★] P. Shah,[3] W. D. Kenworthy,[4] R. Kessler,[5,6] T. M. Davis [7] A. Goobar [4] D. Scolnic [8] M. Vincenzi [9] P. Wiseman [2] R. Chen [10] E. Charleton,[2] M. Acevedo,[8] P. Armstrong,[11] B.M. Boyd [12] D. Brout,[13] R. Camilleri,[7] J. Frieman,[14] L. Galbany [15,16] M. Grayling,[12] L. Kelsey [12] B. Rose,[17] B. Sánchez,[18] J. Lee,[19] A. Möller,[20] M. Smith [21] M. Sullivan [2] N. Shiamtanis,[2] A. Alarcon,[22] S.S. Allam,[14] F. Andrade-Oliveira,[23] S. Avila,[24] D. Bacon,[25] J. Blazek,[26] S. Bocquet,[27] D. Brooks,[3] D. L. Burke,[28,29] A. Carnero Rosell [30,31] J. Carretero [32] R. Cawthon [33] L. N. da Costa,[31] M. E. da Silva Pereira [34] H. T. Diehl,[14] S. Dodelson,[5,6,14] P. Doel,[3] S. Everett,[35] C. Frohmaier [25] J. García-Bellido [36] D. Gruen,[27] G. Gutierrez,[14] K. Herner,[14] S. R. Hinton [7] D. L. Hollowood [37] K. Honscheid,[38,39] D. Huterer,[40] D. J. James,[41,42] N. Jeffrey,[3] K. Kuehn,[41,42,43] O. Lahav,[3] S. Lee,[44,45] C. Lidman [11,44,45] J. L. Marshall,[46] J. Mena-Fernández,[18] F. Menanteau,[47,48] R. Miquel,[49,50] J. Muir,[51,52] J. Myles,[53] R. L. C. Ogando,[54,55] M. Paterno,[14] A. A. Plazas Malagón [28,29] A. Porredon,[24,56] J. Prat [5,57] R.C. Nichol,[58] A. K. Romer,[59] A. Roodman,[28,29] E. Sanchez,[24] D. Sanchez Cid,[23,24] I. Sevilla-Noarbe,[24] E. Suchyta [47,60] M. E. C. Swanson,[47] C. To,[5] D. L. Tucker,[14] A. R. Walker [61] N. Weaverdyck [62,63] and M. Aguena[31,64] (The DES Collaboration)

Affiliations are listed at the end of the paper

Accepted 2026 March 20. Received 2026 March 6; in original form 2025 December 5

ABSTRACT

We present improved cosmological constraints from a re-analysis of the Dark Energy Survey (DES) 5-year sample of Type Ia supernovae (DES-SN5YR). This re-analysis includes an improved photometric cross-calibration, recent white dwarf observations to cross-calibrate between DES and low-redshift surveys, retraining the SALT3 light-curve model and fixing a numerical approximation in the host-galaxy colour law. Our fully recalibrated sample, which we call DES-Dovekie, comprises ∼1600 likely Type Ia SNe from DES and ∼200 low-redshift SNe from other surveys. With DES-Dovekie, we obtain $\Omega_m = 0.330 \pm 0.015$ in flat Lambda-cold dark matter (ΛCDM) which changes Ω_m by -0.022 compared to DES-SN5YR. Combining DES-Dovekie with cosmic microwave background data from *Planck,* Atacama Cosmology Telescope, and South Pole Telescope and the DESI DR2 measurements in a flat w_0w_aCDM cosmology, we find $w_0 = -0.803 \pm 0.054$ and $w_a = -0.72 \pm 0.21$. Our results hold a significance of 3.2σ, reduced from 4.2σ for DES-SN5YR, to reject the null hypothesis that the data are compatible with the cosmological constant. This significance is equivalent to a Bayesian model preference odds of approximately 5:1 in favour of the flat w_0w_aCDM model. Using generally accepted thresholds for model preference, our updated data exhibits only a weak preference for evolving dark energy.

Key words: dark energy – transients: supernovae.

1 INTRODUCTION

Type Ia supernovae (SNe Ia) by virtue of their brightness (∼ −19 mag at peak) and low scatter (∼ 0.15 mag after standardization) provide precise distance measurements at gigaparsec scales. Used to discover the accelerating expansion of the universe in A. G. Riess et al. (1998) and S. Perlmutter et al. (1999) with ∼50 SNe Ia, competitive modern analyses require thousands of SNe (D. Brout et al. 2022b; B. Popovic et al. 2024; D. Rubin et al. 2025). In 2024, the Dark Energy Survey (DES) released (B. O. Sánchez et al. 2024) and analysed (DES Collaboration 2024; M. Vincenzi et al. 2024) their 5-yr sample of ∼ 1600 SNe, the largest

★ E-mail: B.A.Popovic@soton.ac.uk

single-telescope sample of likely SNe Ia used in a cosmology analysis to date. Measurements of baryon acoustic oscillations (BAO), the cosmic microwave background (CMB), and gravitational lensing provide complementary constraints. Jointly, these probes provide impressive measurements on the components and history of the universe (S. Alam et al. 2021; T. M. C. Abbott et al. 2024; DES Collaboration 2026b; DESI Collaboration 2025).

The concordance cosmological model Lambda-cold dark matter (ΛCDM), with the universe composed of a cosmological constant, dark matter, and baryonic matter, has been the *de-facto* cosmological model for the past 25 yr. An empirical way to parametrize deviations from ΛCDM is by the dark energy equation-of-state parameter, $w = P/\rho$, where a cosmological constant Λ corresponds to $w = -1$. A conventional parametrisation for a time-evolving equation of state is $w(a) = w_0 + (1 - a)w_a$, where $a = 1/(1 + z)$ is the scale factor (M. Chevallier & D. Polarski 2001; E. V. Linder 2003). This parametrization is capable of approximating the evolution of a wide variety of physical models (e.g. R. Camilleri et al. 2024; K. Lodha et al. 2025) over the redshift range spanned by SNe.

Until recently, analyses of cosmological data sets (M. Betoule et al. 2014; D. Scolnic et al. 2018; T. M. C. Abbott et al. 2019; D. Brout et al. 2019, 2022b) showed consistency with ΛCDM. However, recent supernova measurements from DES-SN5YR (DES Collaboration 2024) and Union3 (D. Rubin et al. 2025) show $\sim 2.5\sigma$ evidence for time-varying dark energy, on their own or in combination with the CMB (Planck Collaboration VI 2020) and BAO from the Sloan Digital Sky Survey (SDSS, S. Alam et al. 2017).[1] Subsequently, new BAO measurements from the Dark Energy Spectroscopic Instrument (DESI, DESI Collaboration 2025) revealed a $2.8\sigma - 4.2\sigma$ discrepancy with a cosmological constant, depending on the choice of SN Ia sample. DESI results are confirmed by DES BAO,[2] which in combination with DES-SN5YR and the CMB show a 3σ discrepancy from ΛCDM (T. M. C. Abbott et al. 2024; DES Collaboration 2026b).

SN Ia data are vital to these results. While ΛCDM does not provide the best fit to the combination of BAO and CMB data in the absence of SNe Ia, models with constant dark energy but non-zero spatial curvature provide a reasonable alternative fit (S.-F. Chen & M. Zaldarriaga 2025).

The consistency of the preference for evolving dark energy between DES-SN5YR and Union3 is particularly notable, due to the majority of the data being different and the pipelines being independent. Using the DES-SN5YR public data release, G. Efstathiou (2024) noted that the preference for evolving dark energy relies on a very robust relative calibration to within 0.01 mag between SNe Ia across their full-redshift range, involving multiple surveys. Additionally, S. Dhawan, B. Popovic & A. Goobar (2025) have demonstrated a toy model to illustrate how SN Ia systematics could potentially translate into a false preference for evolving dark energy. Accordingly, it is crucial to ensure SN Ia systematics are well understood and treated robustly. In particular, G. Efstathiou (2024) noted differences averaging 0.04 mag between low-z and high-z SN Ia that are common to both the PANTHEON+ and DES-SN5YR data sets. M. Vincenzi et al. (2025) traced these differences, finding that they are expected due to improvements in host-galaxy modelling, light-curve fitting (by the SALT method), and different corrections for selection bias between the two data sets. In particular, the photometrically identified DES-SN5YR data set is more complete, requiring smaller bias corrections for selection than the spectroscopically confirmed PANTHEON+. As such, it may be reasonably argued that results from DES-SN5YR will have less systematic risk than those from the earlier PANTHEON+.

Table 1. A top-level summary of the changes between this work and DES-SN5YR and DES Collaboration (2024). Section 5 goes into more detail on each of these points.

Change	DES-SN5YR	DES-Dovekie
Calibration	Fragilistic	Dovekie
SALT model	SALT3.DES5YR	SALT3.DOV
Cal. uncertainties	Underweighted	Fixed
F99 colour law	Approximate	Exact
Simulations	Generated with SALT3.DES5YR	Regenerated with SALT3.DOV
BAO data	SDSS	DESI DR2
CMB data	*Planck*	*Planck*, ACT-DR6, SPT-3G
Posterior sampler	MCMC	Nautilus

To further investigate the DES-SN5YR results, B. Popovic et al. (2025, hereafter, Dovekie) analysis focused on enhancing the photometric cross-calibration of SN Ia surveys, including the use of new data from the *Hubble Space Telescope* (*HST*, G. Narayan et al. 2019; T. Axelrod et al. 2023; B. M. Boyd et al. 2025) and *Gaia* (Gaia Collaboration 2016, 2023; C. Babusiaux et al. 2023). Within the milieu of the current ΛCDM tension, and discussion of systematic uncertainties such as calibration, Dovekie concluded that a re-analysis of DES-SN5YR with this new cross-calibration was necessary to properly estimate the impact on cosmological parameters.

As part of the DES-SN5YR data release, the software and input files needed to replicate the analysis were included, with the aim of enabling future improvements and re-analyses. However, the data release was incomplete, missing a portion of the systematics. Here, we realize the potential of this release and complete it, conducting a full end-to-end re-analysis of the DES-SN5YR results using the Dovekie calibration solution. This re-analysis includes: (1) verifying the pipeline by reproducing the results of DES-SN5YR and DES Collaboration (2024); (2) retraining the SALT3 model with Dovekie calibration; and (3) re-running the analysis pipeline (e.g. fig 1 in DES-SN5YR) that includes light-curve fitting, photometric classification, bias corrections, construction of the systematic covariance matrix, and cosmology fitting. We have also improved and simplified the interface to the publicly available DES-SN5YR pipeline to encourage future efforts to re-analyse this sample.

After initially reproducing the original DES-SN5YR work, we address an outdated approximation in the implementation of the assumed dust colour law in DES-SN5YR (and AMALGAME and PANTHEON+) and assess its impact before performing our cosmological analysis with our improved calibration and fixed colour law.

Table 1 provides a top-level summary of the changes we make to DES-SN5YR and DES Collaboratio (2024) pipelines, which constitute the 'DES-Dovekie' result. The layout of the paper is as follows. Section 2 provides a brief description of the DES-SN5YR data set, Section 3 describes SN Ia standardization and distance measurements. Section 4 describes cosmology fitting. We choose

[1] https://www.sdss4.org/science/final-bao-and-rsd-measurements
[2] The DES BAO results use photometric redshifts, in contrast to the DESI spectroscopic redshifts.

our range of models to facilitate comparisons with the literature, but discuss alternate parametrizations in this section. Differences between this work and DES-SN5YR are given in Section 5, and a review of our consistency checks is presented in Section 6. This is followed by a description of our systematic uncertainties in Section 7, our *Hubble* diagram in Section 8, and systematic uncertainties in Section 9. Our cosmological results are presented in Section 10, and we present our conclusions in Section 11.

2 DATA

The data we use here is the same as used in the DES-SN5YR analysis, combining high-z measurements of photometrically classified SNe with low-z spectroscopically confirmed samples. All surveys involved have been recalibrated in the Dovekie analysis.

2.1 DES-SN5YR

The DES-SN program ran for 5 yr using the Dark Energy Camera (DECam, B. Flaugher et al. 2015; Dark Energy Survey Collaboration 2016), across ten 3 deg^2 fields; two deep fields extending to 24.5 mag depth per visit in each of the *griz* bands, and eight shallow fields with 23.5 mag depth. Host-galaxy redshifts were acquired with a dedicated follow-up program OzDES on the AAOmega spectrograph (G. A. Smith et al. 2004; C. Lidman et al. 2020). Further details on the specific search strategy and spectroscopic follow-up programs are available in R. Kessler et al. (2015) and M. Smith et al. (2020).

The published DES light curves are measured with the 'Scene Modelling Photometry' pipeline (D. Brout et al. 2019; B. O. Sánchez et al. 2024), simultaneously modelling the SN Ia and host-galaxy fluxes. The DES fluxes include chromatic corrections to account for spectral energy distribution (SED) differences between SNe Ia and calibration stars (J. Lasker et al. 2019) and atmospheric corrections to account for differential chromatic refraction (J. Lee et al. 2023). For the low-redshift samples, we did not update their published photometry.

This work, alongside numerous other fruits of the DES collaboration, resulted in the data and cosmology releases as seen in A. Möller et al. (2022); B. O. Sánchez et al. (2024); and M. Vincenzi et al. (2024). We begin with the same initial sample of $\sim$ 3600 observed transients that were published in B. O. Sánchez et al. (2024), but due to survey cuts our recalibrated data set will not be the same size as DES-SN5YR.

2.2 Low redshift

The DES-SN5YR analysis eschewed some of the older historical samples of SNe Ia at low redshift; instead, the low-redshift anchor is comprised of the Center for Astrophysics CfA3 (M. Hicken et al. 2009), CfA4, (M. Hicken et al. 2012), Carnegie Supernova Project (CSP, K. Krisciunas et al. 2017, comprising the 'low-z' sample), and Foundation (R. J. Foley et al. 2018). Only SNe Ia above $z = 0.025$ were included, mitigating the impact of peculiar velocities, and an additional 1 per cent mag error floor was added to the Foundation sample. In contrast to the photometrically typed SNe in DES, the low-redshift supernovae are all spectroscopically confirmed.

2.3 Host galaxies

The most likely host galaxy for an SN Ia (and therefore the corresponding redshift) is identified in deep-stacked photometry free of SN Ia light (P. Wiseman et al. 2020) with the directional light radius ($d_{\rm DLR}$) method presented by M. Sullivan et al. (2006) and R. R. Gupta et al. (2016). An SN Ia is considered 'hostless' if the $d_{\rm DLR} > 4$, otherwise likely hosts were targeted as part of the previously mentioned OzDES programme (F. Yuan et al. 2015; M. J. Childress et al. 2017; C. Lidman et al. 2020). The efficiencies of these follow-up programs in acquiring a host-galaxy redshift are detailed in M. Vincenzi et al. (2023) and B. O. Sánchez et al. (2024); SNe without a host are not included in our cosmology sample.

The host galaxies are characterized via two global properties: the stellar mass $M_\star$ and the rest-frame $u - r$ colour. These two properties can be computed across the redshift range of the analysis with the limited broad-band photometry. The host-galaxy masses and colours are fit consistently across the surveys using the code, pipeline, and procedure described in M. Sullivan et al. (2010) and the PEGASE2 templates from M. Fioc & B. Rocca-Volmerange (1999) and D. Le Borgne & B. Rocca-Volmerange (2002) with a P. Kroupa (2001) initial mass function. The DES host galaxies are supplemented with photometry from *uJHK* photometry when possible (P. Wiseman et al. 2020; W. G. Hartley et al. 2022), and the low-redshift host photometry from PS1 (Pan-STARRs) is supplemented with ultraviolet photometry from *GALEX* (L. Bianchi, B. Shiao & D. Thilker (2017) and the SDSS $u-$band.

For the low-redshift anchor, updated spectroscopic redshifts are provided by A. Carr et al. (2022); estimated peculiar velocity corrections are provided by E. R. Peterson et al. (2022) with uncertainties set to a uniform 250 km s^{-1} (D. Scolnic et al. 2018).

2.4 Non-Ia classification

Baseline classification of SNe in DES-SN5YR is performed with SuperNNova (SNN, A. Möller & T. de Boissière 2020), a recurrent neural network machine-learning classifier designed to train and operate on photometric SNIa data and host-galaxy redshift. To train SNN, a suite of realistic simulations is generated using SED time-series for core collapse (SN types II, Ib, Ic) and for peculiar 91bg-like and SNIax (R. Kessler et al. 2019; M. Vincenzi et al. 2019), with SNN model parameters optimized for DES in A. Möller et al. (2024).

Alternative classifiers SCONE (H. Qu et al. 2021) and SNIRF (supernova identification with random forest),[3] each with different training and prediction algorithms compared to SNN, are used to assess systematic uncertainties on classification (for more details, see A. Möller et al. 2022; M. Vincenzi et al. 2024).

3 STANDARDIZATION METHODOLOGY

Here, we provide a brief summary of the cosmological inference methodology employed by the DES-SN5YR analysis. Broadly, the BEAMS (Bayesian Estimation Applied to Multiple Species) with Bias Correction (BBC) method (R. Kessler & D. Scolnic 2017, implemented within R. Kessler et al. 2009, 2019, and managed by S. Hinton & D. Brout 2020) uses the light-curve parameters to determine distances, and to apply bias corrections that account for selection effects and non-SNIa contamination. In the cosmology fit, these distances are weighted by their uncertainties and their probability of being a type Ia supernova.

[3] https://github.com/evevkovacs/ML-SN-Classifier

3.1 Light-curve modelling and fitting

To acquire SN Ia distances, we perform multiband photometry fitting of the observed photometry of the SN Ia light curve. DES-SN5YR used the SALT3 model (W. D. Kenworthy et al. 2021), itself an update to the widely used SALT2 model from J. Guy et al. (2010). SALT is a description of the SED of the population of observed type Ia supernovae, similar to a principal component analysis; it is empirically derived from a training sample of spectroscopically confirmed SNe. DES-SN5YR used the G. Taylor et al. (2023) training of SALT3 (hereafter SALT3.DES5YR), which presented four major changes to the previous models used in cosmology: an increased training sample, increased wavelength coverage,[4] the eschewing of observer-frame U band from the training, and the Fragilistic calibration solution from D. Brout et al. (2022a). Here, we use the updated SALT3.DOV model, retrained using the fiducial Dovekie calibration solution. Further, the SALT3.DOV model has cut many SNe measured by legacy surveys from the training sample; the SALT3.DOV model thus continues a trend towards more stringent requirements on calibration.

For a given light-curve fit, there are five parameters used to characterize the SN: redshift z, time of peak brightness T_0, stretch x_1, colour c, and the overall flux normalization x_0, typically used in magnitude units m_B ($m_B = 10.635 - 2.5\log(x_0)$). The best-fitting values and associated uncertainties of each parameter are determined to measure distances; to this end, spectroscopic measurements of the host-galaxy redshift are used ($\sigma_z \sim 10^{-4}$), allowing us to fix the redshift during the light-curve fitting process.

Distances with the SALT model are inferred from the Tripp estimator (R. Tripp 1998)

$$\mu = m_B + \alpha x_1 - \beta c - M_0 - \Delta\mu_{\rm bias} - \delta_{\rm host}, \quad (1)$$

where m_B, x_1, and c are defined as above, M_0 is the peak brightness of a fiducial SN Ia. $\delta_{\rm host}$ is the term that corrects for the 'mass step' (P. L. Kelly et al. 2010; H. Lampeitl et al. 2010; M. Sullivan et al. 2010) that occurs for the standardized brightness of an SN Ia, expressed as a sigmoid function:

$$\delta_{\rm host} = \gamma(1 + e^{(M_\star - S)/\tau_{M_\star}})^{-1} - \gamma/2, \quad (2)$$

where γ is the magnitude of the luminosity difference between those SNe located in 'high' mass galaxies ($M_\star > 10^{10}{\rm M}_\odot$) and 'low mass' ($M_\star < 10^{10}{\rm M}_\odot$) galaxies. S is the step location, nominally set to $S = 10^{10}\,{\rm M}_\odot$, and $\tau_{M_\star}$ is the width of the step. The mass step is accounted for during the BBC process. α, β, and $\Delta\mu_{\rm bias}$ are explained below.

3.2 Bias corrections

The α and β nuisance[5] parameters describe the luminosity–stretch and luminosity–colour relationship, respectively. These nuisance parameters, alongside the luminosity–distance relationship of SNe Ia, can be biased by selection effects arising from the flux-limited nature of SNe Ia observations. The biases arising from these selection effects must be accounted for, and typically this is done via large Monte Carlo simulations that attempt to accurately model detection and other selection effects K. Perrett et al. (2010), M. Betoule et al. (2014), R. Kessler et al. (2019), and B. Popovic et al. (2021).

[4] 2800−8000 Å central filter wavelength compared to 2800−7000 Å.
[5] Not 'nuisance' in the Bayesian sense, as we do not marginalize these parameters.

Following DES-SN5YR, we use the BBC update in B. Popovic et al. (2023) that is compatible with dust models introduced in D. Brout & D. Scolnic (2021), and we use the updated dust parameters from B. Popovic et al. (2023). The simulated $\Delta\mu_{\rm bias}$ term is averaged in 4D cells of $\{z, c, x_1, \log_{10}({\rm M}_\star)\}$:

$$\Delta\mu_{\rm bias} = m_B + \alpha^{\rm true}x_1 - \beta^{\rm true}c - M_0^{\rm true} - \mu^{\rm true}, \quad (3)$$

where parameters noted with the superscript 'true' are the simulated parameters, and m_B, x_1, and c are obtained from SALT3.Dovekie light-curve fits in the same was as for the data.

This 'BBC-4D' approach seeks to ameliorate not only conventional Malmquist bias, wherein more-distant distributions of SNe Ia are biased towards brighter events, but also other biases. Potential biases in x_1 and c are mitigated in the aggregate, unlike 'BBC-1D', which only operates as a function of redshift. Other methods of bias modelling, primarily the Bayesian hierarchical model 'unity' from D. Rubin et al. (2025), are employed in other analyses but return similar cosmological results to BBC.

3.3 Non-Ia contamination

In a cosmology analysis with photometrically classified SNe Ia, a portion of SNe that remain after light-curve fitting quality cuts may not actually be Type Ia. In order to properly account for these contaminants in the cosmology analysis, DES-SN5YR made use of the BEAMS framework from M. Kunz, B. A. Bassett & R. A. Hlozek (2007), R. Hlozek et al. (2012), M. Knights et al. (2013), and implemented in BBC. See M. Vincenzi et al. (2023, 2024) for more information.

4 COSMOLOGY FITTING

4.1 Models and theory

Our baseline model for cosmological distances is the linear parametrization of the dark energy equation of state, given by

$$w = w_0 + w_a(1 - a)\,, \quad (4)$$

and denoted w_0w_aCDM. We opt for this parameterisation (although suboptimal, as w_0 and w_a will in general be correlated, this formulation has now become conventional). We define the curvature density parameter $\Omega_{\rm k}$ as $\Omega_{\rm m} + \Omega_\Lambda = 1 - \Omega_{\rm k}$, and refer to $\Omega_{\rm k} = 0$ as flat. We omit the radiation density as negligible for late-times. Then, flat ΛCDM is a special case of flat w_0w_aCDM with $w_0 = -1$ and $w_a = 0$, and flat wCDM means $w_a = 0$ but w_0 is allowed to vary from -1. We collectively denote the cosmological model parameters as $\Theta = (\Omega_{\rm m}, \Omega_\Lambda, w_0, w_a)$ where $\Omega_{\rm m}$ is the matter density parameter today.

A potentially more informative description of the equation of state is given by (w_p, w_a) where

$$w = w_p + w_a(a_p - a)$$

and a_p is defined as the scale factor where the variance of $w(a)$ is minimized, or equivalently where w_p and w_a are uncorrelated. As explained in E. V. Linder (2007), it is expected to be the case that when including CMB data that $a_p \sim 0.4$, nevertheless this parametrisation may be interesting for some data combinations.

The transverse comoving distance χ is

$$\chi(z_{\rm cos}) = \frac{c}{H_0}\frac{1}{\sqrt{|\Omega_{\rm k}|}}\,\sinh\left(\sqrt{|\Omega_{\rm k}|}\int_0^{z_{\rm cos}}\frac{{\rm d}z}{E(z)}\right), \quad (5)$$

where $z_{\rm CMB}$ is the redshift in the rest frame of the CMB (the frame in which the dipole would be absent), and $\mathrm{sinn}(x) = \sin(x), x, \sin h(x)$ depending on $\Omega_{\rm k} < 0, \Omega_{\rm k} = 0, \Omega_{\rm k} > 0$ respectively. $E(z) \equiv H(z)/H_0$ is the normalized redshift-dependent expansion rate and

$$H(z) = \left[\Omega_{\rm m}(1+z)^3 + \Omega_{\rm k}(1+z)^2 + \Omega_\Lambda(1+z)^{3(1+w_0+w_a)}e^{-3w_a z/(1+z)}\right]^{1/2} \quad . \tag{6}$$

The luminosity distance is given by

$$D_l(z_{\rm obs}, z_{\rm CMB}) = (1+z_{\rm obs})\chi(z_{\rm CMB}) \quad , \tag{7}$$

where $z_{\rm obs}$ is the observed heliocentric redshift, which captures the effect of beaming due to peculiar velocity of both the Sun and the SN Ia with respect to the CMB rest frame. The distance modulus is $\mu(z, \Theta) = 5\log_{10}(D_l(z, \Theta)/10\ \mathrm{Mpc}) + 25$.

We compute the difference between data and theory for every ith supernova, $\Delta\mu_i = \mu_{{\rm obs},i} - \mu(z_i, \Theta)$, and write the likelihood $\mathcal{L}$ in the standard form

$$-2\log\mathcal{L} \equiv \chi^2 = \Delta\mu_i \mathcal{C}^{-1}_{ij}\Delta\mu^T_j \quad , \tag{8}$$

where $\mathcal{C}^{-1}$ is the inverse covariance matrix (including both statistical and systematic errors) of the $\Delta\mu$ vector, and the methodology of computing $\mathcal{C}_{\rm syst}$ follows the approach described in M. Vincenzi et al. (2024):

$$\mathcal{C}^{ij}_{\rm syst} = \sum_{S=1}^{N_{\rm syst}} (\Delta\mu^i_{{\rm obs,S}})(\Delta\mu^j_{{\rm obs,S}})W_S^2 \tag{9}$$

where changing systematic parameter S gives differences in SN Ia distances $\Delta\mu$. Indices i, j are iterated over all the SNe in the analysis (i, $j = 1...N_{\rm SNe}$) and W_S is the weight for each systematic (which is set to 1 unless otherwise stated).

A potential source of confusion in cosmology with SN Ia is that the absolute magnitude of the fiducial SN Ia (M_0) and the H_0 parameter (which appears in the luminosity distance) are completely degenerate. They may be combined in the single parameter $\mathcal{M} = M_0 + 5\log_{10}(c/H_0)$. Our results are marginalized over $\mathcal{M}$.

For our nominal cosmology, we use the COSMOSIS[6] package from J. Zuntz et al. (2015) with the NAUTILUS[7] nested sampler (J. U. Lange 2023).

4.2 Combination with other cosmology probes

We combine our DES SNe constraints with those from other complementary probes.

(i) *Cosmic microwave background.* We use the measurements of temperature and polarization power spectra (TTTEEE) from Planck Collaboration V (2020), in combination with ground-based measurements from the Atacama Cosmology Telescope (ACT) and the South Pole Telescope (SPT). We also include lensing reconstructions in our analysis. Specifically, we combine the `simall` and `Commander` likelihoods for $\ell < 30$, with the `Plik-lite` likelihood for $\ell < 1000$, 600 (TT, and TE, EE respectively) as wrapped in the PYTHON implementation `Planck-py` [8] (H. Prince & J. Dunkley 2019). To this, we add TTTEEE data implemented in the `ACT-DR6-Lite` [9] likelihood (T. Louis et al. 2025; S. Naess et al. 2025), and SPT-3G data (E. Camphuis et al. 2025) as wrapped in the `candl` likelihood (L. Balkenhol et al. 2024).[10] Our lensing likelihoods are the `actplanck-baseline`,[11] option based on the combined ACT and *Planck* lensing reconstruction maps (J. Carron, M. Mirmelstein & A. Lewis 2022; M. S. Madhavacheril et al. 2024; F. J. Qu et al. 2024), together with SPT-3G lensing (Z. Pan et al. 2023) again implemented in `candl`. This forms a comprehensive and up-to-date account of CMB data, and it extends that used in both DES Collaboration (2024) and DESI Collaboration (2025) by including both ACT and SPT. While there is a small ℓ overlap between ACT and *Planck,* and a small sky area overlap between ACT and SPT that may cause their constraints to not be fully independent, it has been argued that the overlap is not material to cosmological analysis (E. Camphuis et al. 2025; T. Louis et al. 2025). We comment on the influence of the choice of CMB data further in the results section.

(ii) *Baryonic acoustic oscillations.* We use data from DESI DR2 as presented in DESI Collaboration (2025). DESI DR2 measures the apparent size of BAO both along and perpendicular to the line of sight of various tracers in redshift bins ranging from $0.3 < z < 2.3$. These act to constrain expansion models between the distance between the CMB and the relevant redshift.

4.3 Model preference

To interpret our parameter constraints, we test the relative preference of extended models for our full range of data compared to flat ΛCDM.

There has been some debate in the community as to appropriate metrics for model preference, with some authors preferring frequentist methods (e.g. DESI Collaboration 2025), and others preferring Bayesian evidence (e.g. DES Collaboration 2024). For both methodologies, preference is primarily driven from the goodness-of-fit improvement $\Delta\chi^2$. The difference between the two can then be largely attributed to the penalty applied to the complex model, or equivalently appropriate thresholds against which to judge significance.

Frequentist methods evaluate relative probabilities of data, not models. As per DESI Collaboration (2025), we apply Wilk's Theorem[12] (S. Wilks 1938). This states that the logarithm of the ratio of the maximum-likelihood (ML) probability of the same data in each model follows a χ^2-distribution with degrees of freedom (d.o.f.) equal to the number of additional parameters in the extended model (one in the case of wCDM and two for w_0w_aCDM). We determine the ML for each model and the difference $\Delta\chi^2_{\rm ML}$ between the extended model and flat ΛCDM (by construction a positive value), and convert to a p-value with the χ^2-distribution. We then express the p-value as a number of sigma, $n\,\sigma$, by solving

$$\mathrm{CDF}_{\Delta\chi^2}(\log p \mid \mathrm{d.o.f.}) = \frac{1}{\sqrt{2\pi}}\int_{-n}^{n} e^{-t^2/2}\mathrm{d}t \quad . \tag{10}$$

In this case, the complex model penalty is relatively lenient, appearing as the degrees of freedom in the χ^2-distribution.

[6] https://github.com/joezuntz/cosmosis
[7] https://github.com/johannesulf/nautilus
[8] https://github.com/heatherprince/planck-lite-py
[9] https://github.com/ACTCollaboration/DR6-ACT-lite
[10] https://github.com/Lbalkenhol/candl
[11] https://github.com/ACTCollaboration/act_dr6_lenslike
[12] Strictly only approximate for real data, as terms of $\mathcal{O}(1/\sqrt{N})$ where N is the number of data points are neglected.

Bayesian methods consider directly the relative confidence of models, given the data. The evidence ratio R_{01} is defined as

$$R_{01} = \frac{p(M_0|D)}{p(M_1|D)} \ , \tag{11}$$

where M_0 is flat ΛCDM and M_1 is the extended model, and D is the data. Given an agnostic a-priori preference for either model, $\log R_{01} = \Delta \log \mathcal{Z}$ where the evidence $\mathcal{Z}$ of each model is

$$\mathcal{Z} = \int p(D|\Theta, M) p(\Theta|M) d\Theta \ , \tag{12}$$

which has explicit dependence on the a priori confidence in the model parameters $p(\Theta)$. In this case, the complex model penalty is approximated by the relative compression between the a priori and a posteriori probability volumes (see e.g. D. Sivia & J. Skilling 2006). $\log \mathcal{Z}$ is computed by NAUTILUS as part of the sampling process. Although NAUTILUS does not compute errors in this statistic, we have tested alternative samplers, NAUTILUS settings and choices of random seed for initialization, and estimate our error to be $\sigma(\log \mathcal{Z}) \sim 0.2$. We interpret $\Delta \log \mathcal{Z}$ on the scale defined in table I of R. Trotta (2008), as used by DES Collaboration (2024).

The arbitrariness of Bayesian priors has been sometimes given as a reason to prefer frequentist methods. However, reasonable prior confidence intervals can be set based on broad astrophysical considerations; for example, a minimum age for the universe based on stellar ages. If there is a decisive model preference, the widths of the priors (so far as they remain reasonable) will not be a determining factor. We quote both metrics.

For the Bayesian evidence calculations, we adopt uniform priors $H_0 \in (0.55, 0.91)$, $w_0 \in U(-3, -0.4)$, $w_a \in U(-3, 2)$, $\Omega_k \in (-0.15, 0.15)$, and $\Omega_m \in (0.1, 0.5)$. As is conventional, we also require $w_0 + w_a < 0$.[13] For the CMB, we adopt $\Omega_b \in (0.03, 0.07)$, $\tau \in (0.01, 0.2)$, $10^9 A_s \in (0.5, 5.0)$ and we fix the sum of neutrino masses at $\Sigma m_\nu = 0.06$ eV. The CMB normalization nuisance parameter priors are $A_{\rm Planck} \sim \mathcal{N}(1.0, 0.0025)$, $P_{\rm ACT} \sim \mathcal{N}(1.0, 0.003)$, $E_{\rm cal} \sim \mathcal{N}(1.0, 0.0095)$, $T_{\rm cal} \sim \mathcal{N}(1.0, 0.0036)$, and $A_{\rm foreground} \in (0.0, 2.0)$ (as recommended in E. Camphuis et al. 2025) and we fix the remaining ACT normalization parameter $A_{\rm ACT}$ to $P_{\rm ACT}$ as ACT is calibrated off *Planck*.

While our priors are broadly consistent with DESI Collaboration (2025), there are a few differences. First, we have lowered the upper limit on Ω_m from 0.9 to 0.5 because $\Omega_m > 0.5$ is inconsistent with a wide range of other galaxy surveys. Secondly, the upper limit on w_0 is set to avoid confusing dark energy with other components of the energy density such as curvature or matter. Thirdly, the prior on Ω_k is tighter than typically adopted. This more restrictive prior reduces compute time to acceptable levels, and is consistent with the evidence to date in favour of a Universe that is close to spatially flat. Our posteriors are wholly contained within priors, except for some SN-only cases. In this instance, we quote parameter constraints on broadened priors, while retaining the above priors for the evidence calculations.

5 DIFFERENCES TO DES-SN5YR

In the introduction, we briefly mentioned a mistake in the implementation of the E. L. Fitzpatrick (1999) colour law. SNANA was using a polynomial expansion centred at $R_V = 3.1$, which was accurate to < 1 per cent for this assumed R_V value but for simulations of bias corrections where a multitude of R_V are used, the error is larger. This mistake was identified in the process of other work within SNANA, and replaced with the full E. L. Fitzpatrick (1999) colour law. This change has negligible impact on the data with the assumed $R_V = 3.1$ for Milky Way extinction. There is a measurable impact on simulated bias corrections as described in Appendix A.

Dovekie performed a recalibration of historically used samples of SNe Ia, including the low-redshift surveys used within the DES-SN5YR analysis. While Dovekie uses the same overall framework as the DES-SN5YR calibration solution (Fragilistic; D. Brout et al. 2022a) using the all-sky PS1 telescope[14] as interstitial observations, Dovekie improves on this methodology in a number of ways:

(i) The addition of DA white dwarfs from B. M. Boyd et al. (2025), combining extensive modelling of these white dwarf spectra with direct observations from DES, PS1, and the SDSS.
(ii) The use of *Gaia* spectroscopy as a complementary method to characterize published filters by integrating spectra through filter transmission functions, alongside filter transmission measurements with PS1.
(iii) Subtle improvements to error modelling in the cross-calibration.
(iv) Separate improvements to the SALT training and error models.

In addition to a changed set of calibration offsets, Dovekie solved for filter shifts, finding changes to the following filters that directly impact the DES-SN5YR cosmology analysis: CfA3K-V, CSP-B/V, and every filter in CfA4P1/2. The +30 Å shift to the PS1 g band in Fragilistic was reverted to its published J. L. Tonry et al. (2012) value. These new filter changes, from fits to survey photometry, alongside the new calibration offsets from Dovekie, were used to train a new SALT model.

These improvements, alongside the other system changes, have resulted in changes to the zero-points of surveys within the DES-SN5YR sample. We show the changes, as a function of the median redshift of the survey, in Fig. 1. A more thorough overview of this new calibration, and potential changes, is presented in Dovekie.

We repeat the DES-SN5YR cosmology analysis with this new calibration solution and SALT model, SALT3.DOV. We regenerate the 'biasCor' files (Section 3) with the new SALT model, filters, and calibration offsets. Furthermore, we redo the DES-SN5YR light-curve fits with this new SALT model and calibration.

Additionally, during the course of this reanalysis, we found a minor error in the weighting (equation 11 in DES-SN5YR) of the photometric uncertainty systematics. This error arose from a mistake in the input file,[15] rather than an issue with the equation or methodology, and caused the weights of the calibration systematic to sum to 0.81 instead of 1. This resulted in a reduction of the estimated total photometric uncertainty by ~ 20 per cent for DES-SN5YR. We correct this mistake.

[13] $w_0 + w_a < 0$ is justified in the literature as necessary to ensure there is a period of matter-domination in the early universe (necessary for growth of structure).

[14] DES does not have sufficient sky-coverage overlap with low-redshift surveys, which precludes its use here as the interstitial.

[15] Specifically, the weight on each of the 9 SALT3 calibration variants was mistakenly rounded to 0.3 instead of the correct value of $1/\sqrt{9} = 0.33$.

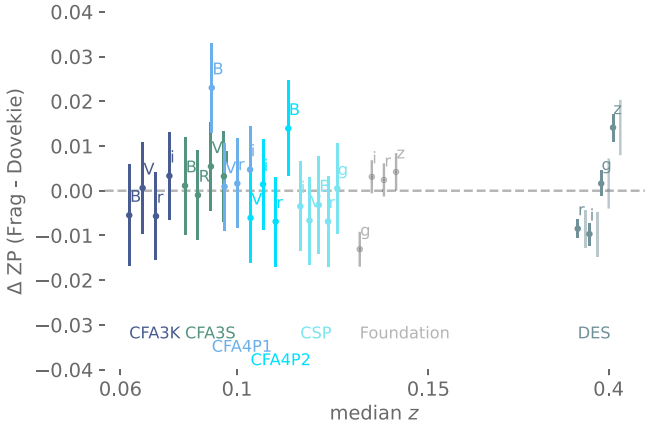

Figure 1. The DES-SN5YR sample includes the DES, CfA3S, CfA3K, CSP, and Foundation; the difference in calibration offsets for each filter and each survey is plotted at the approximate median redshift of the survey. To demonstrate the improvement in precision with the new calibration, the light vertical bars show the calibration uncertainties for DES without using the nominal DA WD. The mean zero-point across all surveys has been subtracted out for both Dovekie and Fragilistic, for visual clarity.

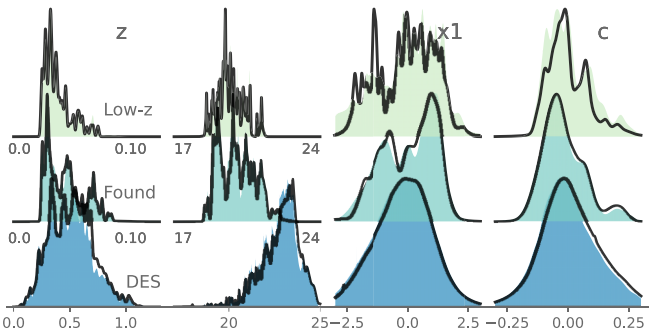

Figure 2. Distributions of z, m_B, x_1, c for DES-SN5YR (black) and this work (filled histogram). We split the sample into its constituent parts, DES (bottom; blue), Foundation (middle; teal), and Low-z (top; light green). We see agreement between the two analyses, with the exception of the DES c distribution.

Finally, we modify the cut on $\sigma_{x_1} < 1.0$ from DES-SN5YR to $\sigma_{x_1} < 1.15$. Due to changes in error propagation between SALT3.DES5YR and the new SALT3.DOVEKIE, the x_1 errors were generally increased relative to other light-curve fitting parameters. We choose the new $\sigma_{x_1} < 1.15$ cut to preserve the 20 per cent quantile cut established in DES-SN5YR.

To summarize:

(i) *Updated E. L. Fitzpatrick (1999) colour law.* During unrelated work within SNANA,[16] it was discovered that the implementation of the E. L. Fitzpatrick (1999) colour law term within SNANA was a polynomial expansion centred at $R_V = 3.1$. The full F99 colour law was implemented, and it was discovered that this impacted simulated and inferred distance moduli on the order of ~ 0.01 mag, though primarily impacting the simulated bias corrections.

(ii) *Updated calibration.* We use the updated cross-calibration solution from Dovekie, in place of Fragilistic. While the zero point offsets between the two are largely similar, they notably differ for DES.

(iii) *Updated SALT model.* Fragilistic combined the estimation of calibration uncertainties with those of the SALT modelling, which provided more reliable estimations of systematic uncertainty arising from the two. This necessitates a retraining of the SALT model with the new calibration solution.

(iv) *Regenerated bias correction simulations.* Table 6 highlights the specific systematic uncertainties that are regenerated, and therefore directly impacted, by this re-analysis.

(v) *Fixed calibration uncertainties.* As previously stated, DES-SN5YR used an incorrect weight of $\psi = 0.3$ for each of the systematic SALT surfaces. This caused DES-SN5YR to underestimate the photometric uncertainty by ~ 20 per cent. We update this to the more correct value of 0.33.

[16]See Appendix A.

Table 2. KS test for consistency between DES-Dovekie and DES-SN5YR, for SALT3 parameter distributions and for each subsample.

Parameter	Difference Between DES-Dovekie and DES-SN5YR		
	σ (DES)	σ (Foundation)	σ(Low-z)
z	0.0σ	0.0σ	0.0σ
c	2.8σ	0.0σ	0.2σ
x_1	1.2σ	0.2σ	0.0σ
m_B	0.3σ	0.0σ	0.0σ

6 CONSISTENCY CHECKS

In this section, we review the changes in SN Ia parameters between this work and the original DES-SN5YR analysis, and investigate the source of any changes and their potential impact.

6.1 DES-SN5YR and this work

Fig. 2 shows the z, m_B, x_1, and c distributions for the DES-SN5YR data set, fit with SALT3.DES5YR and Dovekie. DES-SN5YR contained 1829 SNe total, compared to our 1820 SNe. Within DES, we report 1623 likely ($P_{\rm SNIa} > 0.5$) SNe Ia, compared to 1635 SNe Ia in DES-SN5YR. At low redshift, we have 197 SNe compared to 194 in DES-SN5YR. We find 1718 overlapping SNe between DES-SN5YR and DES-Dovekie, with approximately 100 different SNe between the two analyses. We find that supernovae passing fits with Dovekie not previously included in DES-SN5YR appear to be consistent with the overall x_1/c populations; they are not bluer, redder, or from any particular stretch distribution. Table 2 shows the likelihood, presented in σ discrepancy of a Kolmogorov–Smirnov (KS) test, that selected parameters are drawn from different distributions between DES-SN5YR and this work.

As expected, the distributions least sensitive to calibration (x_1, z) show no significant divergence at the population level. The only distribution that is significantly modified is the colour distribution among DES SNe; this is principally a shift in the mean of the distribution from $\bar{c} = 0.011$ to -0.003. To compare the shapes of the colour distributions, we remove the $\bar{c}$ shift and redo the KS test; this reduces the significance of the difference to 1.6σ, as evaluated by bootstrap resampling. This colour shift is not surprising; colour is highly sensitive to calibration, and the mean of the colour distribution is determined by the demographics of

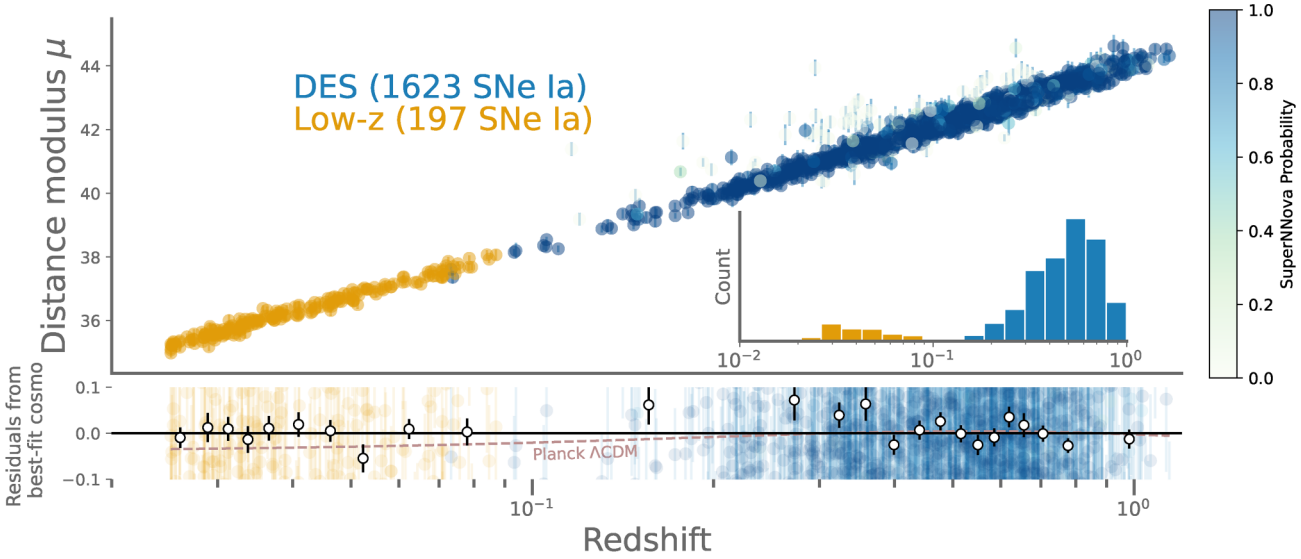

(a) Hubble diagram of DES-Dovekie. DES is shown in blue, with low-redshift supernovae in orange. For each DES event, the classification probability from SNN is indicated by the colour. **Upper:** Full Hubble diagram. **Lower:** Hubble residuals from best-fit $w_o w_a$CDM cosmology. The Planck Collaboration et al. (2020b) cosmology is shown in light maroon dashed line. **Inset:** Redshift histogram of the two subsamples.

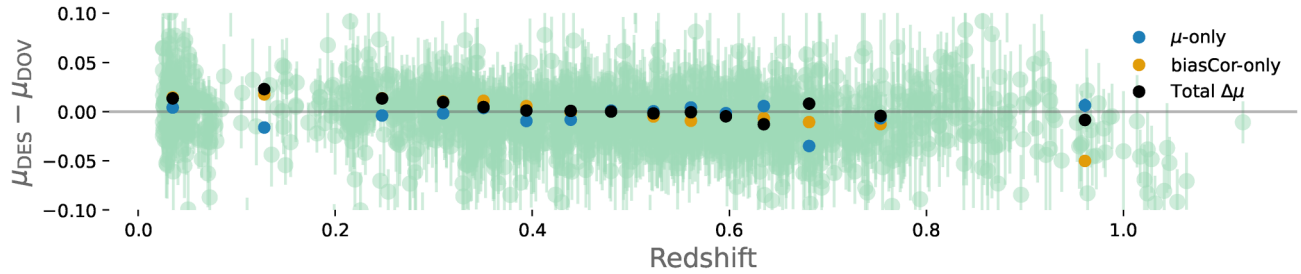

(b) The difference between the DES-SN5YR published distances and DES-Dovekie distances. The error-weighted average $\Delta\mu$ in black includes shift in μ *and* the change in bias-correction. We show the un-bias-corrected μ averages in blue, and the bias-correction component alone in orange.

Figure 3. The DES-Dovekie *Hubble* diagram, and the change in inferred, bias-corrected μ values between DES-SN5YR and this work.

the SALT training sample. The calibration of the low-z surveys is mixed, resulting in no coherent offset. The overall changes in distance are shown in Fig. 3, but detailed further in Section 8.

6.2 Internal consistency

BBC relies on good agreement between the simulated bias corrections and observed data for an unbiased cosmology analysis. To accurately model intrinsic brightness in simulated bias corrections, DES-SN5YR used the best-fitting parameters from DUST2DUST (B. Popovic et al. 2023), which describes populations of stretch, colour, $M_\star$, A_V, and R_V.

To check if the existing DUST2DUST model is valid in the DES-Dovekie analysis, we compare our data with our new SALT3.DOV simulations. Fig. 4 shows the overlaid distributions of z, m_B, x_1, c, $M_\star$ for data and the new biasCor simulations; we see good agreement between data and simulations, and find no distribution that disagrees at more than 3σ. Given the consistency of the data-sim comparisons, we have chosen to use the same DUST2DUST model that was used in DES-SN5YR.

The final consistency check is to test our ability to recover our simulated cosmology parameters from performing the full analysis on 25 statistically independent simulated samples. To avoid excessive CPU consumption using Cosmosis on 25 samples, we use a faster and simpler minimization code[17] that replaces the full *Planck* likelihood with a parametrization using the CMB R-shift parameter as described in B. O. Sánchez et al. (2022). Averaging results of the 25 samples for a flat wCDM cosmology with a CMB prior, we recover our input cosmology, flat ΛCDM with $\Omega_m = 0.315$, to under 1σ for both parameters: $w_{reco} = -0.9986 \pm 0.0045$ and $\Omega_{m,reco} = 0.316 \pm 0.001$. When fitting for the $w_0 w_a$CDM cosmology, we similarly recover our input cosmology using CMB priors: $w_{0,reco} = -1.0027 \pm 0.0223$ and $w_{a,reco} = -0.0325 \pm 0.1015$.

6.3 Unblinding criteria

Through the course of this analysis, we blinded cosmological parameters estimated from real data until certain unblinding criteria were met. Pipeline validation, as in DES-SN5YR, was performed on realistic and detailed catalogue-level simulations, which were fit to test the recovery of simulated cosmology parameters.

We follow the unblinding criteria laid out by DES-SN5YR:

(i) *Recovery of original DES-SN5YR cosmology parameters.* To ensure that any measured changes in cosmology arise from the

[17] https://github.com/RickKessler/SNANA/blob/master/src/wfit.c

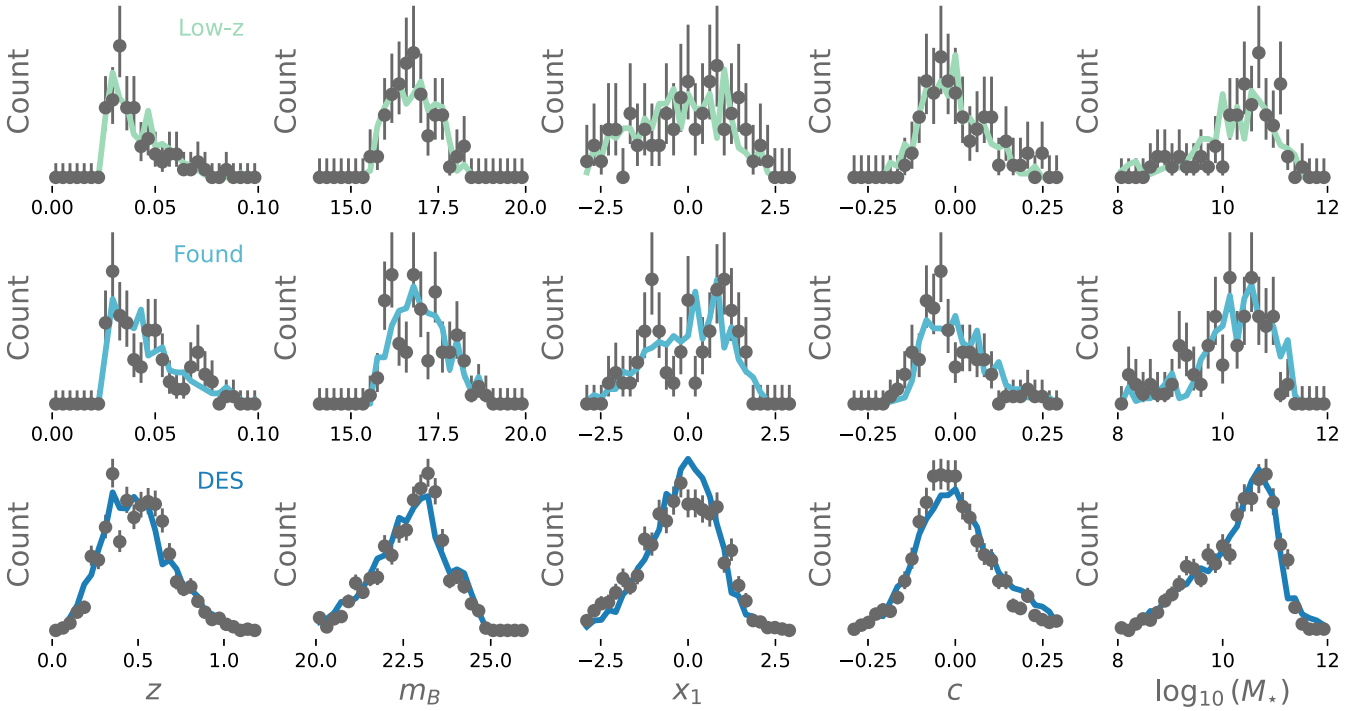

Figure 4. Comparison between the simulated and observed SN Ia parameters. The data are presented in grey points, and the simulations are presented in coloured histograms.

changes in Table 1, and not from changes in the pipeline since the publishing of DES-SN5YR, we repeat the original DES-SN5YR analysis using the same (current) SNANA code that is used in this re-analysis. For this test, a flag was added to the SNANA code to restore the E. L. Fitzpatrick (1999) colour law bug, and we restored the mistaken calibration weight.

(ii) *Recovery of input simulated cosmology.* We produce 25 statistically independent simulacra of the DES-SN5YR data set assuming a flat ΛCDM cosmology. Each of the 25 simulations is run through our analysis pipeline and fit with a CMB prior for wCDM and w_0w_aCDM cosmology.

(iii) *Accuracy of simulations.* Following DES-SN5YR, test the accuracy of our simulations across our observables. Specifically, we test $z, x_1, c, m_B, M_\star, \mu - \mu_{\rm model}$, and the redshift and host-galaxy mass evolution of x_1 and c, and require a reduced χ^2 between data and simulations to lay between 0.7 and 3.0.

Additionally, we provide a brief summary of the consistency and improvement tests that Dovekie performed during their analysis to ensure a good calibration solution:

(i) *Recovery of simulated offsets.* Dovekie simulated 100 catalogues of tertiary stars with a random ZP offset for each survey. They recovered their simulated offsets within 1σ across their 100 simulacra.

(ii) *Updated DES-SN5YR tertiary stars.* Dovekie increased the number of tertiary stars used for the cross-calibration by a factor of 2.

(iii) *Consistency between DA WD and tertiary stars results.* The DES $g-r$ shift in Fig. 1 is consistent between the calibration results with DA WD modelling and with the conventional tertiary star approach.

(iv) *Hubble residual scatter.* Dovekie found equal or improved Hubble Residual scatter with their new calibration and SALT surface.

7 DESCRIPTION OF SYSTEMATIC UNCERTAINTIES

Here, we briefly summarize the sources of systematic uncertainty considered in DES-Dovekie. A more full description is available in DES-SN5YR; we follow their choices of systematic uncertainty. The covariance matrix for each systematic is calculated from equation (9), and each $\mathcal{C}$ term is computed from a light-curve fitting and BBC process.

7.1 Calibration

To evaluate the calibration contributions to $\mathcal{C}$, we use the nominal SALT model with calibration from Dovekie, to draw nine systematic SALT surfaces randomly from the covariance matrix derived during the cross-calibration. Accordingly, we set $W_S = 1/\sqrt{9} = 0.33$, such that the quadrature sum of our SALT surface systematics is 1.

An additional source of uncertainty, related to the CALSPEC flux calibration, is considered, with a shift of 5 mmag/7000 Å (as recommended in R. C. Bohlin, K. D. Gordon & P.-E. Tremblay 2014) applied to the data.

7.2 SN Ia properties and astrophysics

The nuisance parameters α, β, γ in equation (1) are assumed to be constant in the nominal analysis. However, a redshift evolving nuisance parameter, such as $\alpha(z) = \alpha_0 + \alpha_1 \times z$, may capture unmodelled evolution of SN Ia parameters. As a systematic, we allow α, β, and γ to separately evolve with redshift with the same

linear relation as above. We also perform a fit with a fixed $\alpha = 0.16$, and $\beta = 3.1$, to estimate the impact of the lower β found in photometric data compared to spectroscopic data.

The location of the mass step is placed at $\log_{10} M_\star = 10$ in our nominal analysis. However, reflecting the uncertainty in both measurements of the stellar mass of host galaxies and the uncertainty of the nature of the mass step, we test the impact of moving the location of the mass step 'split' to the median of the sample, at $\log_{10} M_\star = 10.3$.

During the PANTHEON+ analysis, updates to the the intrinsic scatter $\sigma_{\rm int}$ definition were implemented, redefining it as

$$\sigma^2_{\rm floor}(z_i, c_i, M_{*,i}) = \sigma^2_{\rm scat}(z_i, c_i, M_{*,i}) + \sigma^2_{\rm gray}, \quad (13)$$

which is a function of the $c, z, M_\star$ parameters, as opposed to the original BBC methodology which did not include $M_\star$-dependence.

We revert to this constant $\sigma_{\rm int}$ model as a source of systematic uncertainty, to test the impact of this colour-dependent scatter term compared to the historical grey intrinsic scatter.

The largest source of systematic uncertainty in DES-SN5YR was the nature of SN Ia scatter. The D. Brout & D. Scolnic (2021) model introduced the concept of SN Ia scatter being driven by differing dust distributions in the host galaxies of SNe Ia. Improved by B. Popovic et al. (2023), the systematic uncertainty test for DES-SN5YR was derived using three sets of dust parameters drawn from the chains of DUST2DUST. Additionally, a version of the D. Brout & D. Scolnic (2021) model with adjusted parameters (specifically the τ parameters do not match BS21) was included, though the provenance of these changes has been lost. We include this systematic.

Finally, the nominal analysis uses the host-galaxy stellar mass $M_\star$ as the tracer to explain correlations between the SNe Ia and their host environment. While the host-galaxy stellar mass is the host property most robust to limited photometric information, it is not necessarily the most accurate tracer of SN Ia brightness. Following P. Wiseman et al. (2022), which proposes that the $u - r$ host-galaxy colour may instead be the driving factor in these correlations, we incorporate an alternative model labelled as 'W22', with a 'colour step' analagous to the mass step.

The W22 model utilizes SNe rates and delay time distributions from P. Wiseman et al. (2022) to drive galaxy evolution including stellar age, mass, and star formation rate, which is then correlated to the SNe Ia properties via the relationships via N. Nicolas et al. (2021).

7.3 Milky Way extinction

Given the importance of the dust distributions of other galaxies, we consider the impact of our own Milky Way galaxy. The SALT3 fitting code includes Galactic extinction in the model fluxes; inaccurate extinction modelling can bias the SALT3-fitted colours.

We consider two systematics associated with the Milky Way corrections. The first is a global scaling of 5 per cent down of the E. F. Schlafly & D. P. Finkbeiner (2011) values, following D. Brout et al. (2022b). The second systematic is a change from the E. L. Fitzpatrick (1999) reddening law to that presented from J. A. Cardelli, G. C. Clayton & J. S. Mathis (1989).

7.4 Host and survey modelling

Simulations of SNe Ia within the SNANA framework draw from a realistic catalogue of galaxies to model the observed SN-host correlations in the data. While the nominal catalogue is generated from DES co-added images from P. Wiseman et al. (2020) and H. Qu et al. (2024), we test an additional, shallower catalogue ('SVA Gold'), based on DES science verification data, used in other DES analyses: R. Kessler et al. (2019) and M. Smith et al. (2020).

Further, we test the systematics of our selection function. We model the efficiency of obtaining the spectroscopic redshift of a host galaxy as a function of host-galaxy brightness, $\epsilon_z^{\rm spec}$ (M. Vincenzi et al. 2023), which helps model the selection effects of the DES survey. The systematic test we apply is to shift this function to observe host-galaxy $r-$band brightness that are $+0.2$ and -0.2 mag fainter and brighter, respectively. Their weights are $W_S = \sqrt{1/2}$ each.

7.5 Contamination and photometric classifiers

Compared to analyses with spectroscopically confirmed SNe Ia, DES included non-Ia contamination within the sample, potentially biasing the distances via the use of non-standardizable SNe. The nominal analysis uses the SNN classifier by A. Möller & T. de Boissière (2020), which had been rigorously tested by M. Vincenzi et al. (2023).

The systematic analysis of the core-collapse contamination comes in three parts: simulated Ia+non-Ia training set, modelling the Core Collapse prior in BBC with simulated sample, and the classifier method.

The nominal analysis used the simulations of non-Ia SNe developed by M. Vincenzi et al. (2019); this is replaced for systematic tests by the templates and simulations from D. O. Jones et al. (2017), hereafter J17, and additionally real-data observed in DES, hereafter 'DES-CC'.

To evaluate the uncertainty on classification method, SNN was replaced with two alternate classifiers: SCONE (H. Qu et al. 2021) and SNIRF. These classifiers are trained on the same set of simulations that the nominal SNN model was trained on. Additional training sets were also used for systematics.

Each of these approaches relies on a suite of simulations of non-Ia SNe to inform the BEAMS method about populations; a final systematic test for BBC is to replace the simulated non-Ia prior with a redshift-dependent polynomial fit as described in R. Hlozek et al. (2012).

7.6 Redshift

A coherent redshift shift of 4×10^{-5} is applied to the data, following J. Calcino & T. Davis (2017), to test for the impact of a local void or other such redshift errors.

To correct for peculiar velocities, we use corrections from 2M++; our systematic uncertainties come from approaches implemented in E. R. Peterson et al. (2022). The first is to maintain the 2M++ corrections, but integrate over the line of sight between the distance and the redshift. Secondly, we switch to the peculiar velocity map from the 2MASS Redshift Survey (2MRS, R. Lilow & A. Nusser 2021). Both systematics are weighted such that they sum in quadrature to 1.

8 RESULTS

8.1 Reproducing DES-SN5YR

The results of DES-SN5YR were unblinded in 2023, and in the intervening years, SNANA has introduced updates to the light-curve fitting, simulating, and cosmology-fitting programs that were originally used in DES-SN5YR. To check if the changes in

Table 3. Nuisance parameters from DES-Dovekie analysis, the original V24 analysis, and simulated data corresponding to DES-Dovekie.

Sample	$N_{\rm SNe}$	α	β	γ	RMS
Simulations	1605	0.140	2.80	0.0	0.158
Data – DES-SN5YR	1829	0.170(1)	3.12(3)	0.038(7)	0.168
Data – DES-Dovekie	1820	0.169(3)	3.14(3)	0.033(8)	0.169
DES	1679	0.17(1)	3.17(4)	0.04(1)	0.165
Foundation	118	0.15(1)	2.9(14)	0.015(23)	0.110
Low-z	83	0.15(1)	2.88(14)	−0.009(30)	0.120

cosmology that we measure are solely due to changes in Table 1, and to ensure consistency in our pipeline across time, we attempt to replicate the published results of DES-SN5YR. This attempt to recreate DES-SN5YR 'as-published', dubbed 'Lyrebird', will be used to track and identify major changes to SNANA that have shifted the final cosmology results. This Lyrebird test uncovered two additional changes: a code fix to the E. L. Fitzpatrick (1999) colour law (Appendix A), and an input mistake in the systematic weight for calibration. The Lyrebird test includes the F99 code bug and the incorrect calibration weight.

Because of the potential code and pipeline changes, and the use of up-to-date data and likelihoods for the CMB and BAO, we do not expect Lyrebird to recover the exact same cosmological parameters as DES Collaboration (2024). However, we have checked that our Lyrebird results are compatible with the results published in the DES Key Paper and DESI DR2 (DESI Collaboration 2025). A summary of our recovered Lyrebird cosmology is given in Table 4; for this table, we take the published DES-SN5YR distances and covariance and use a quick-fitting solution, replacing the full CMB likelihood with distance priors derived from the results of P. Lemos & A. Lewis (2023). We find agreement in all cases within $\ll 1\sigma$.

8.2 The DES-Dovekie *Hubble* diagram

Fig. 3 presents the DES-Dovekie *Hubble* diagram. We find 1623 DES likely SNe Ia, and 197 SNe Ia at low redshift. Our low-redshift sample has three additional events compared to DES-SN5YR, and our DES sample has nine fewer events. Table 5 provides a breakdown on the quality and survey cuts we perform.

Table 3 provides the final nuisance parameters α, β, γ, and the *Hubble* residual RMS, for the DES-Dovekie data and 25 simulated data sets, alongside a summary of the equivalent values for DES-SN5YR. While we have a slightly smaller sample, the nuisance parameters remain unchanged between DES-SN5YR and DES-Dovekie. None the less, analysis of DES-Dovekie simulations maintain the same curious $\beta = 2.8$ as DES-SN5YR.

Table 5. Number of SN Ia remaining after quality and survey cuts.

Requirement	Low-z	DES SN DES	Total
SALT3 fit	376	3590	3991
$\lvert x_1 < 3 \rvert \& \lvert c < 0.3 \rvert$	313	2818	3196
$\sigma_{x_1} < 1.15, \sigma_{t_{\rm peak}} < 2$	304	2259	2628
Valid host z	291	1710	2066
Chauvenet's criterion	207	1682	1943
Valid bias corrections	201	1680	1881
Common SNID	197	1623	1820
Total	197	1623	1820

9 SYSTEMATIC UNCERTAINTIES

We assess the systematic uncertainties here, and compare to those in DES-SN5YR, with the systematic uncertainties impacted by the Dovekie calibration highlighted in green. As per DES-SN5YR, we analyse systematics in the context of the flat wCDM model, using the fast cosmology fitter wfit, returning to more sophisticated models and fitters for the cosmology solution.

Table 7 gives the values of the individual systematic uncertainties, for SNe alone without any priors. As in DES-SN5YR, we remind the reader that the individual systematic uncertainties do not sum to the total systematic uncertainty. We evaluate each individual contribution with a 'leave-one-out' approach, comparing the uncertainty with and without a given systematic. With the all sources of systematic uncertainty considered, internal correlations between systematics partially cancel out during the fitting process. This is not the case during the leave-one-out approach, and therefore the systematic uncertainties do not sum to the total systematic uncertainty. In a similar vein, the δw ($w_{\rm stat+syst} - w_{\rm stat}$) values in Table 7, which are generated with an 'add-one-in' approach, do not match the total change in w. Remembering the internal correlations within the cosmology fitting process, it is not surprising that several of the systematic uncertainties have shifted with regards to DES-SN5YR.

First, we show the error budget for $\Omega_{\rm m}$ in a flat ΛCDM universe for SNe Ia alone in Fig. 5. We present the equivalent error budget but for flat wCDM in Fig. 6 with and without a CMB prior, which we shall focus on for this section.

Table 4. Comparison of cosmological parameters, between the published DES Collaboration (2024) distances and the recreation of those distances, nicknamed Lyrebird in this work. We pick data combinations that are most informative for comparison: in flat ΛCDM, SN Ia only data is used, flat wCDM uses SN+CMB, and Flat w_0w_aCDM uses SN+CMB+DESI BAO. The values for the original distances are not expected to exactly match those in DES Collaboration (2024) as the BAO and CMB likelihoods have been updated, and fitting uses the NAUTILUS sampler. The minor changes in sample composition do not affect the cosmology solution.

Parameter	Original DES-SN5YR distances	Lyrebird
$\Omega_{\rm m}$ (flat ΛCDM)	$+0.352 \pm 0.017$	$+0.357 \pm 0.017$
w (flat wCDM)	-0.934 ± 0.027	-0.927 ± 0.027
$\Omega_{\rm m}$ (flat wCDM)	$+0.330 \pm 0.009$	$+0.331 \pm 0.008$
w_0 (flat w_0w_aCDM)	-0.770 ± 0.060	-0.760 ± 0.060
w_a (flat w_0w_aCDM)	-0.740 ± 0.220	-0.750 ± 0.230
$\Omega_{\rm m}$ (flat w_0w_aCDM)	$+0.318 \pm 0.006$	$+0.319 \pm 0.006$

Table 6. An overview of the systematics in DES-SN5YR and this re-analysis. Those systematics that are directly impacted by the recalibration in Dovekie are marked with a star ∗.

Baseline	Weight	Systematic	Label
Calibration and light-curve modelling			
SALT3 surfaces and ZP	1/10	10 covariance realizations	'SALT3+Calibration'
HST Calspec 2020 update	1	5 mmag/7000 Å	'HST Calspec'
SN Ia properties and astrophysics			
Dust-based model B. Popovic et al. (2023) ('P23($M_\star$)')∗	1/3	3 realizations from MCMC dust model fitting code	'P23 dust pop 1/2/3'
	1	Original BS20 dust parameters	'BS21'
	1	Splitting on $u-r$	'P23($u-r$)'
Empirical modelling of x_1–$M_\star$ correlations∗	1	Modelling SN Ia age following P. Wiseman et al. (2022)	'Model SN Ia age'
Fixed α/β	1	$\alpha=0.16, \beta=3.1$	'Fixed α/β'
No α evolution	1	$\alpha(z)=\alpha_0+\alpha_1\times z$	'α evolution'
No β evolution	1	$\beta(z)=\beta_0+\beta_1\times z$	'β evolution'
No γ evolution	1	$\gamma(z)=\gamma_0+\gamma_1\times z$	'γ evolution'
Mass step location at 10^{10}M$_\odot$	1	$10^{10.3}$M$_\odot$	'Mass location'
$\sigma_{\rm int}$ modelling with scaling+additive scatter terms (equation 13)	1	Scaling term only	'$\sigma_{\rm int}$ modelling'
Milky Way extinction			
MW scaling E. F. Schlafly & D. P. Finkbeiner (2011)	1	5 per cent scaling	'MW scaling'
MW colour law R_V=3.1 and F99	1/3	R_V=3.0 and CCM	'MW colour law'
Host and survey modelling			
SN Ia host catalogue by H. Qu et al. (2024)∗	1	SN Ia host catalogue using SVA Gold galaxy catalogue	'DES SV catalogue'
Efficiency $\epsilon_z^{\rm spec}$ presented by V21∗	1	Shift of ±0.2 mag in the efficiency curves	'Shift in host spec eff'
Contamination and photometric classifiers			
Classification using SNN	1	SCONE, SNIRF	
Classifier training sample simulated using V19 templates	1	J17 templates, DES CC templates ('SNN training')	
Core-collapse SN prior using V19 simulation	1	Polynomial fit as in R. Hlozek et al. (2012)	'CC SN prior'
Redshift			
Peculiar velocities using 2M++	1	2M++(line-of-sight integration) or 2MRS	'Pec velocities'
No redshift shift	1/6	$\Delta z=4\times10^{-5}$	'Redshift shift'

9.1 Calibration and light-curve modelling

We find that the combined systematic uncertainty that describes calibration and SALT training, σ_w(phot) has increased from DES-SN5YR, going from 0.057 to 0.075 in our analysis. However, the comparable σ_w(phot) values hides noticeable changes between this work and DES-SN5YR. The relative weights from DES-SN5YR have been changed to no longer underestimate the photometric calibration uncertainties (as in Section 5). We find a SALT3+Calibration uncertainty in w of only 0.066, compared to 0.052 in DES-SN5YR. Taking into account the increase of ~ 20 per cent from the change in relative weights, we see the Dovekie photometric uncertainty is consistent with DES-SN5YR.

Fig. 7 shows the impact on the bias-corrected μ for the nine sets of distance moduli used to assess the systematic uncertainty. We see no obvious trend with redshift.

9.2 SN Ia properties and astrophysics

SN Ia properties and astrophysics remains the largest source of systematic uncertainty to-date, approximately ×2 the size of calibration and light curve modelling. We find a slight decrease of 0.009 in σ_w(Astro) over DES-SN5YR, though this is not driven by any particular one systematic.

9.2.1 *Dust systematics*

The dust systematics – P23 dust pop 1–3, P23($u-r$), BS21, and W22 – represent the largest grouping of systematic uncertainties for astrophysics in SNe Ia at σ_w(dust) = 0.101. Table 8 shows the $\delta\chi^2$ for these systematics; none of them are particularly favoured over the nominal P23 model. Noticeably, the largest $\delta w = 0.029$ is from the P23($u-r$), which has no contribution to the total systematic uncertainty – likely indicating that this particular systematic does not well match the data.

9.2.2 *Nuisance parameter systematics*

The remaining properties/astrophysics systematics relate to SN Ia nuisance parameters α, β, γ, $\sigma_{\rm int}$ and the changes to their redshift evolution and initial properties. Interestingly, there is a slight preference to a $\gamma(z)$ at $-1.6\chi^2$, and a $-0.5\chi^2$ change when changing our initial estimations of α and β. Overall, these nuisance parameters contribute to our error budget but are subdominant to the suite of dust systematics. $\sigma_{\rm int}$ as a function of redshift is provided in Fig. 8.

9.3 Milky Way extinction systematics

We find a marginal increase to the Milky Way extinction systematics; given the consistency between Milky Way extinction

Table 7. Systematic uncertainties considering SN-only, without a CMB prior. More detail on each systematic is given in Section 9 and Table 6. Bolded numbers are the sum of each individual component. For comparison, we present the σ_w values from DES-SN5YR. Unlike in Table 8, the δw presented here use the full covariance matrix as presented in Section 3.

Systematic	σ_w	Per cent (tot)	δw	DES-SN5YR σ_w
Total Stat+Syst	0.142	100	0	0.152
Total Statistical	0.11	N/A	−0.092	0.132
Calibration and LC model	**0.075**	14.4 per cent	–	**0.057**
SALT3+Calibration	0.066	12.6	−0.073	0.052
HST Calspec	0.009	1.8	-0.001	0.006
SN Ia astrophysics	**0.124**	23.9 per cent	–	**0.133**
P23 dust pop 1	0.006	1.1	0.001	0.019
P23 dust pop 2	0.021	4.1	−0.004	0.024
P23 dust pop 3	0.025	4.8	−0.009	0.020
P23$(u-r)$	0.0	0.0	0.029	0.00
Dust model as in BS21	0.029	5.6	−0.007	0.027
Model SN age (W22)	0.02	3.8	−0.008	0.00
Fixed $\alpha\beta$	0.0	0.0	0.0	0.002
αevolution	0.013	2.6	−0.002	0.020
β evolution	0.0	0.0	−0.001	0.000
γevolution	0.003	0.6	−0.0	0.011
Mass step location	0.0	0.0	0.0	0.000
$\sigma_{\rm int}$ modelling	0.007	1.3	−0.0	0.013
Milky Way extinction	**0.041**	7.7 per cent	–	**0.034**
MW 5 per cent scaling	0.024	4.5	−0.011	0.020
MW colour law CCM	0.017	3.3	−0.006	0.014
Survey modelling	**0.002**	0.4 per cent	–	**0.015**
DES SV catalogue	0.0	0.0	0.006	0.009
Shift $\epsilon_z^{\rm spec}$	0.002	0.4	0.0	0.005
Contamination	**0.018**	3.5 per cent	–	**0.028**
Classifier SCONE	0.003	0.6	−0.0	0.006
Classifier SNIRF	0.002	0.3	0.0	0.013
SNN different training	0.01	2.0	−0.001	0.006
Core-collapse SN prior	0.003	0.6	−0.001	0.003
Redshift	**0.040**	7.8 per cent	–	**0.037**
Redshift shift	0.011	2.2	−0.0	0.012
Peculiar velocities	0.029	5.6	−0.016	0.025

systematics between Dovekie and Fragilistic, this is not surprising.

9.4 Host and survey modelling systematics

Fig. 9 shows the two 'survey modelling' systematics, changing the host spectroscopic efficiency 'shift $\epsilon_z^{\rm spec}$' and swapping the host library for the SVA Gold catalogue. We find the systematic uncertainty from both tests is consistent with 0. Fig. 9 shows the $\Delta\mu$ for these host systematics.

9.5 Contamination and photometric classifier systematics

Following Milky Way extinction and survey modelling, we find small reductions to the systematics associated with contamination. The total systematic uncertainty is marginally smaller than DES-SN5YR, and there appears to be some migration between the sources of uncertainty – our uncertainty due to SNN alternative training is now 0.010, compared to 0.006 in DES-SN5YR.

9.6 Redshift systematics

Finally, we consider our redshift systematics, which have slightly increased from DES-SN5YR; this change is driven by an increased uncertainty from the peculiar velocities.

10 COSMOLOGY

Here, we present our constraints on cosmological parameters for DES-Dovekie (our nominal data set with updated calibration and colour law) for four models in particular: flat ΛCDM, ΛCDM, flat wCDM, and flat w_0w_aCDM, with four different sets of probes: SN-only, SN+CMB, SN+BAO and SN+CMB+BAO. We reviewed our external probes in Section 3, but as a reminder CMB refers to the combination of *Planck* (Planck Collaboration VI 2020), ACT (T. Louis et al. 2025), and SPT (E. Camphuis et al. 2025) temperature and polarization spectrum (TTTEEE) and lensing reconstruction data, and BAO refers to DESI DR2 measurements as described in table IV of DESI Collaboration (2025). We summarize our results in Table 10. The values we quote are medians throughout, with the error bars representing the 16 per cent and 84 per cent percentiles.

In Appendix B, we present the changes to DES Collaboration (2024) arising solely from the changes to the F99 colour law. Comparisons of DES-Dovekie to DES-SN5YR are shown in Appendix C.

10.1 Data consistency

It is well known that combining data that are in tension (according to some suitable metric) within a given model results in

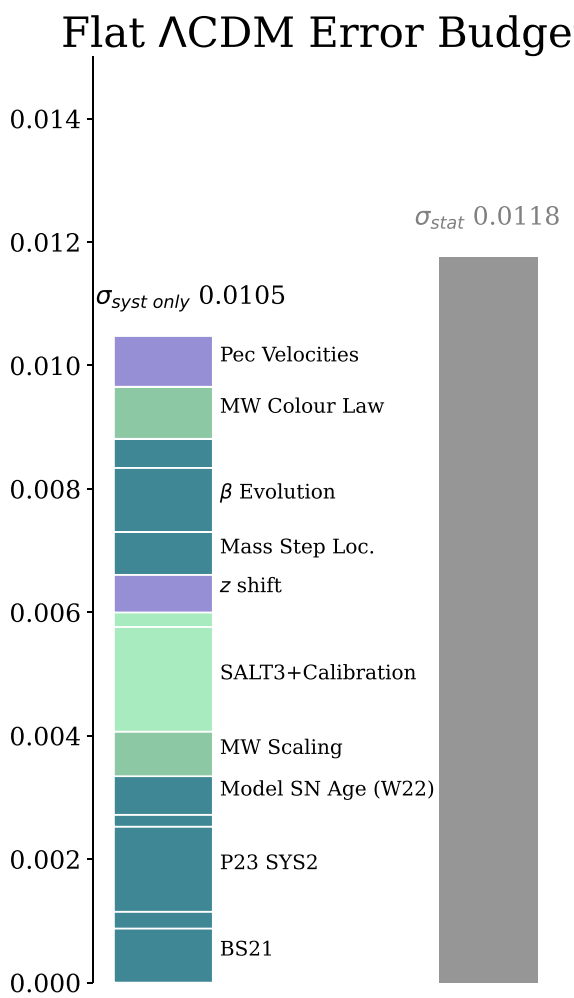

Figure 5. Systematic and statistical error budget on Ω_m for a flat ΛCDM cosmology with SNIa only. Systematics are colour coded as in Fig. 6, and only significant ($\sigma_{sys} > 0.005$) systematics are labelled. The statistical error is presented in grey.

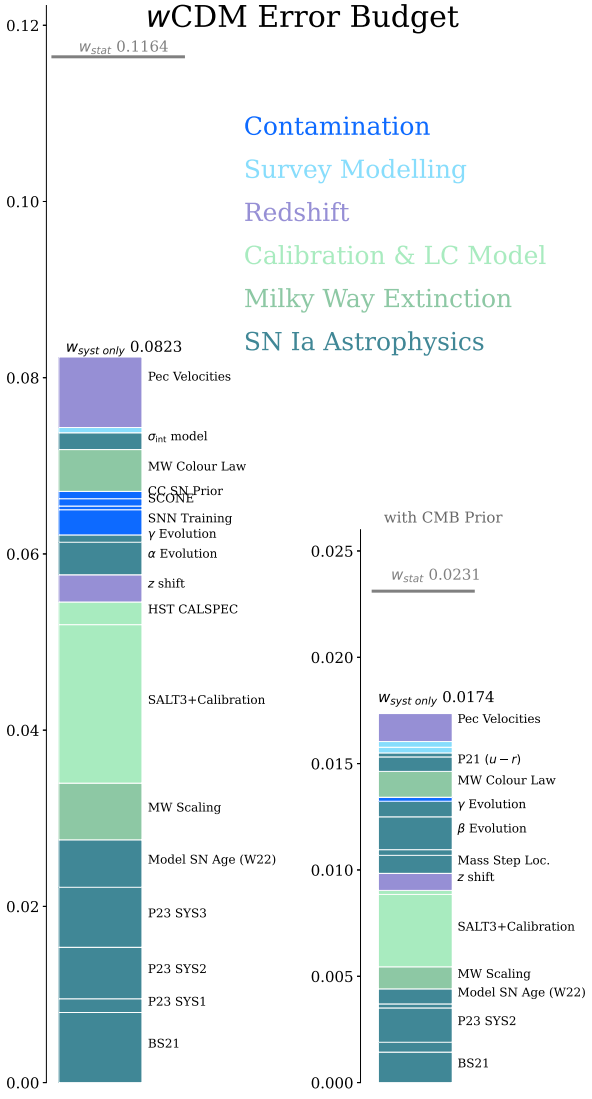

Figure 6. Systematic and statistical uncertainty budget on w, both with (right) and without (left) a CMB prior. Each box is scaled by the total systematic uncertainty. Those systematic uncertainties that are not labelled with text represent a negligible (<0.005) systematic contribution.

artificially tight parameter constraints in the standard analysis. We check that DES-Dovekie is compatible with CMB, BAO, and the BAO+CMB combination using the suspiciousness statistic as described in W. Handley & P. Lemos (2019). Suspiciousness is defined as

$$\log S = \log R - \log I \,, \tag{14}$$

where the R statistic

$$\log R = \log \mathcal{Z}_{AB} - \log \mathcal{Z}_B - \log \mathcal{Z}_B \tag{15}$$

is defined from the relative evidences of the combination of data sets A and B, that is the ratio of the probability of B knowing A compared to the probability of B (in a given model). The evidence $\mathcal{Z}$ was defined in equation (12). The R statistic is prior-dependent so the term

$$\log I = \mathcal{D}_A + \mathcal{D}_B - \mathcal{D}_{AB} \tag{16}$$

is subtracted to remove this. $\mathcal{D}_A$ is the Kullbeck–Leibler divergence of data set A

$$\mathcal{D}_A = \left\langle \log \frac{\mathcal{P}_A}{\pi} \right\rangle_{\mathcal{P}_A} , \tag{17}$$

which quantifies the gain in information from the prior parameter distribution π to the posterior $\mathcal{P}$. We choose S as it is defined via integrals in information-theoretic terms, and is therefore re-parametrization invariant (and so robust in the case of non-Gaussian distributions, which an important feature here). It also works with the entire parameter space rather than a subset, so tensions cannot be concealed or exaggerated by projection effects.

We use the criteria described in W. Handley & P. Lemos (2019) to evaluate a data combination: $\log S > -2.5$ is compatible, $-5 < \log S < -2.5$ is moderate tension, and $\log S < -5$ is strong tension. The S statistic is χ^2-distributed so we also convert S to an equivalent $n\sigma$.

10.2 Flat ΛCDM

In Fig. 10, we show the Ω_m posteriors for DES-Dovekie, CMB and BAO, with data combinations presented in Table 10. For

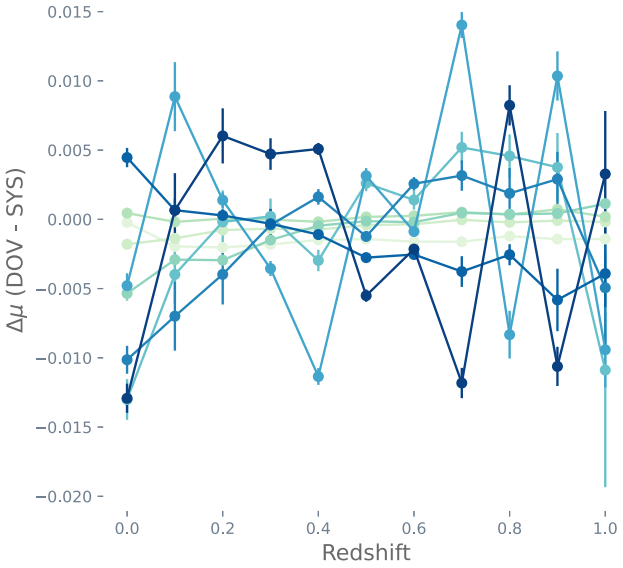

Figure 7. The median binned differences between the nominal distances and the none calibration systematics (colour coded for each systematic surface) for DES-Dovekie. Comparable to Fig. 10 in Dovekie, though we observe no obvious redshift-dependence.

DES-Dovekie, we find an

$$\Omega_m = 0.330 \pm 0.015(\text{SNonly}),$$

which is consistent with CMB results. Adding CMB data results in

$$\Omega_m = 0.317 \pm 0.005(\text{SN} + \text{CMB})$$

which is 1.9σ from DESI DR2 which has $\Omega_m = 0.297 \pm 0.009$.

For the combination of DES-Dovekie with BAO+CMB, $\log S = -1.05$ which is a p-value equivalent to 1.7σ. Hence, we judge it reasonable to combine all three data sets which results in

$$\Omega_m = 0.3045 \pm 0.0032(\text{SN} + \text{CMB} + \text{BAO}).$$

With the addition of CMB data, we also find the *Hubble* constant as $H_0 = 68.14 \pm 0.23\,\text{km s}^{-1}\,\text{Mpc}^{-1}$, and discuss this further in Section 11.3.

10.3 Open ΛCDM

Fitting DES-Dovekie to a universe with non-zero spatial curvature, we find

$$\Omega_k = 0.14 \pm 0.15\ ,$$

where for this constraint we widen our priors to encompass the full posterior. For the SN+BAO combination, we have $\Omega_k = 0.054^{+0.033}_{-0.036}$, and SN+CMB gives $\Omega_k = -0.0063 \pm 0.0037$. The full combination of SN+BAO+CMB results in

$$\Omega_k = 0.0026 \pm 0.0011(\text{SN} + \text{BAO} + \text{CMB}),$$

and $\log S = -0.97$ for DES-Dovekie compared to BAO+CMB.

As the last of these combinations may at first sight indicate a weak preference for non-zero spatial curvature, we comment on this further in Section 11.2. We illustrate our results in Fig. 11.

10.4 Flat *w*CDM

Fitting DES-Dovekie to flat-wCDM, we find

$$\Omega_m,\ w = 0.263^{+0.064}_{-0.078},\ -0.838^{+0.130}_{-0.142}(\text{SNonly}).$$

DES-Dovekie remains consistent with a cosmological constant at $\sim 1.5\sigma$, as shown in Fig. 12. As noted in R. Camilleri et al. (2024), for SN Ia the partial degeneracy between w and Ω_m approximately follows a line of constant deceleration parameter $q_0 = -\ddot{a}a/\dot{a}^2(z = 0)$. For SN, we find

$$q_0 = -0.423^{+0.063}_{-0.073}\ .$$

When we combine SN Ia with external probes, we get more precise constraints on our cosmological parameters due to the orthogonal degeneracy directions. Combining with the CMB, we find $\Omega_m, w = 0.322 \pm 0.007, -0.978 \pm 0.024$ with $\log S = -1.55$ (1.9σ). When combining with BAO, we find $\Omega_m, w = 0.297 \pm 0.008, -0.909^{+0.035}_{-0.037}$.

Finally, with SN+CMB+BAO, we find

$$\Omega_m,\ w = 0.305 \pm 0.005,\ -0.995^{+0.019}_{-0.020}(\text{SN} + \text{BAO} + \text{CMB})$$

and $q_0 = -0.537 \pm 0.026$. While our w constraint might be interpreted that the full data indicates a Universe consistent with a cosmological constant, E. V. Linder (2007) has pointed out that values close to $w = -1$ follow from the inclusion of CMB data, almost irrespective of the data at low redshift (see eqs 1–3 and following paragraph of text in E. V. Linder 2007). Furthermore, in this case $\log S = -2.87$ (2.5σ), indicating the data are not compatible in this model: the tightness of these constraints should be treated with skepticism.

There is no data combination in which flat-wCDM is preferred to flat-ΛCDM in Bayesian evidence.

10.5 Flat w_0w_aCDM

Finally, we present our cosmological fits to flat w_0w_aCDM cosmology. Our SN-only contours are broad with

$$w_0, w_a = -0.50^{+0.35}_{-0.27}, -7.5^{+3.6}_{-4.5}(\text{SNonly}),$$

where for this run only, we have enlarged the w_0w_a priors to encompass the full range of significant posterior probability. The wide range of this posterior reflects the degeneracy in the low-redshift *Hubble* diagram between changes to Ω_m and evolving dark energy. As in ΛCDM, our constraining power increases as we combine with other probes which help determine Ω_m; we find

$$w_0, w_a = -0.769 \pm 0.100, -0.98^{+0.47}_{-0.49}$$

for SN+CMB, and

$$w_0,\ w_a = -0.803 \pm 0.054,\ -0.72 \pm 0.21(\text{SN} + \text{CMB} + \text{BAO}).$$

Looking at the pivot redshift, for SN-only we find $z_p = 0.52$ with $w_p = -1.01 \pm 0.13$. It is not entirely expected that we find w close to -1 at the pivot, and we interpret this as re-inforcing the point that DES-Dovekie is entirely compatible with ΛCDM. For SN+BAO we get $w_p = -0.908 \pm 0.036$, and the suspiciousness statistic $S = -1.86$ (1.8σ) indicates this combination is reliable. While this hints at a departure from ΛCDM, the evidence is not very strong. Finally, the combination of SN+BAO+CMB gives $z_p = 0.57$ with $w_p = -0.981 \pm 0.022$ as expected; we emphasize that this is due to compatibility of CMB with ΛCDM, almost independently of late-time evolution.

Table 8. Nuisance parameters and quality of fit changes.

Systematic	BBC parameters			Fit quality		Cosmology	
	α	β	γ	$\sigma_{\rm int}$	RMS	$\delta\chi^2$	Δw
None	0.169(3)	3.14(4)	0.033(8)	0.035	0.170	0.0	0.000
BS21	0.169(4)	3.21(4)	0.021(9)	0.053	0.170	−1.5	−0.003
DUST1	0.168(3)	3.21(4)	0.041(8)	0.050	0.170	1.0	+0.000
DUST2	0.167(3)	3.08(4)	0.026(9)	0.030	0.171	7.0	+0.003
DUST3	0.167(4)	3.09(4)	0.037(9)	0.046	0.171	23.2	−0.001
Model SN Ia Age (W22)	0.168(4)	3.12(4)	0.038(8)	0.045	0.170	1.4	−0.002
New α/β guess	0.179(3)	3.37(4)	0.034(8)	0.039	0.170	−0.5	0.000
αevolution	0.164(6)	3.15(4)	0.033(8)	0.030	0.170	1.1	+0.001
β evolution	0.169(3)	3.08(8)	0.033(8)	0.035	0.170	2.1	−0.006
γ evolution	0.169(3)	3.15(4)	0.04(2)	0.035	0.170	−1.6	+0.000
$\sigma_{\rm int}$ model	0.168(4)	3.13(4)	0.031(9)	0.113	0.170	3.0	0.000
DES SV Catalogue	0.16813(1)	3.1248(3)	0.035(8)	0.036	0.170	3.2	+0.001
INTRSC COLOUR	0.164(4)	3.15(4)	0.029(8)	0.050	0.172	38.4	+0.005
MW scaling	0.169(4)	3.14(4)	0.035(8)	0.030	0.170	2.1	−0.003
HST CALSPEC	0.168(4)	3.15(4)	0.034(8)	0.036	0.170	−1.1	−0.000
MW colour law	0.170(4)	3.14(4)	0.035(8)	0.030	0.170	−0.7	−0.003

Note: Errors on α, β, and γ are shown in parentheses.
Δw is the w-shift relative to the baseline without systematic uncertainties using a 'add-one-in' approach.
$\delta\chi^2$ shows the change in χ^2 relative to baseline.
$\sigma_{\rm int}$ is calculated as in equation (13) such that the reduced $\chi^2 = 1$.

Table 9. Significance of change in cosmological parameter when only considering the calibration systematic uncertainty, for SN+CMB+BAO flat w_0w_aCDM cosmology.

Parameter	Significance ($\sigma_{\rm syst}$)
w_0	1.1σ
w_a	1.2σ

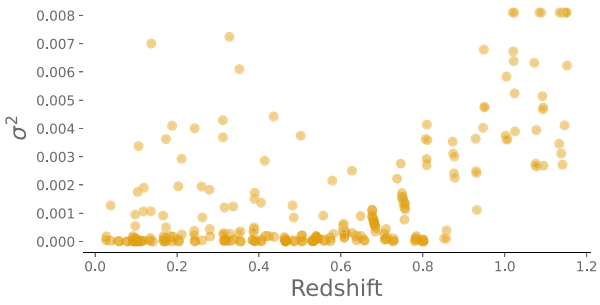

Figure 8. The calculated $\sigma_{\rm int}$ values as a function of redshift.

We show the contours for SN-only, SN+CMB, and SN+CMB+BAO in Fig. 13. An interesting feature of broadening the (w_0, w_a) priors for SN-only is that the overlap of the SN and CMB+BAO contours now appears to arise in a low-probability region of the SN contours.[18] Checking the suspiciousness statistic, we find $\log S = -2.02$ (1.8σ), indicating the data combination is reasonable. A further cross-check of the full posterior reveals that large negative values of w_a are associated with $\Omega_{\rm m} > 0.4$: SN-only data are currently not very good at restricting the extended parameter space of flat w_0w_waCDM.

[18]This probably accounts for why this was not discussed in DESI Collaboration (2025), where the effect must surely have been larger for DES-SN5YR, as only the narrower set of priors were used.

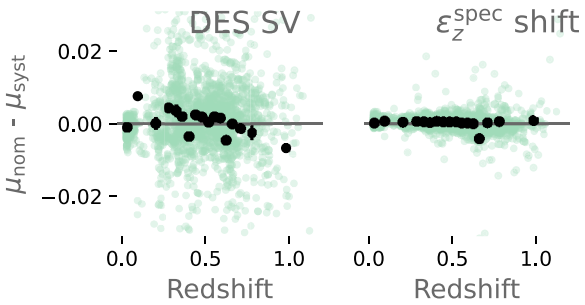

Figure 9. Effects of different survey modelling systematics on the inferred SN Ia distances. Left: choosing a shallower galaxy catalogue (DES 'SVA Gold'). Right: varying the efficiency of obtaining a spectroscopic redshift. Green points are individual realizations, and black points are binned means.

Hence, we interpret the visual appearance of the contours as largely a volume effect of the prior. Furthermore, a narrower prior (which would increase compatibility by shifting the posterior up in w_a) could be argued for on the basis of constraints on $\Omega_{\rm m}$ arising from data not used in this analysis, for example cosmic shear (e.g. DES Collaboration 2026a).

Our final cosmological results are summarized in Table 10, and we discuss the implications for evolving dark energy in Section 11.4. For DES-Dovekie, the number of data points is 1684 which is the effective number of SNe obtained by summing the BEAMS probabilities.

10.6 Cosmological model preference

Following our cosmological fits, we assess the preference of the data for models beyond flat ΛCDM. As explained in Section 3, we use two different metrics. One is frequentist (following DESI Collaboration 2025), deriving from the relative probability of the data between two models, and expressed as an equivalent σ following

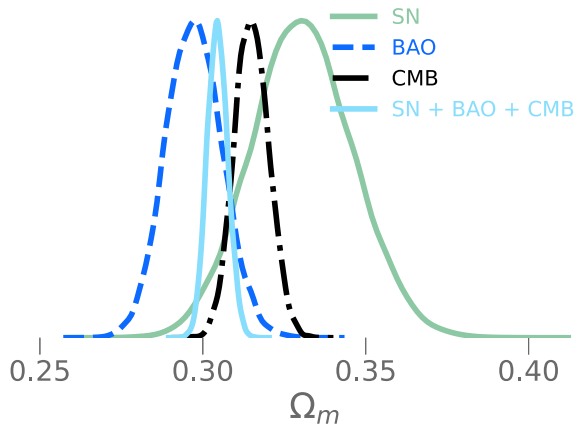

Figure 10. Constraints on the matter density for flat ΛCDM for DES-Dovekie (green), *Planck* CMB (black), DESI DR2 BAO (blue), and the combination SN+CMB+BAO (light blue).

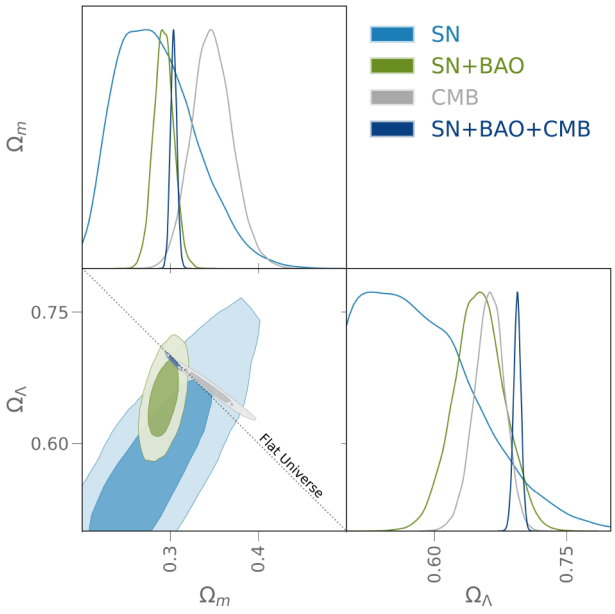

Figure 11. The Ω_m, Ω_Λ contours for open ΛCDM. DES-Dovekie contours are in blue, complemented by the CMB (grey) and SN+BAO (olive) constraints. The full combination of SN+BAO+CMB is in dark blue. As a visual guide, we show the flat universe $\Omega_m + \Omega_\Lambda = 1$ as a dotted line. Although the SN contours appear truncated in this figure (to aid seeing the SN+BAO+CMB data combination), they are derived from our parameter constraints which are quoted with a broadened prior encompassing the full posterior.

equation (10). The other is the Bayesian evidence (following DES Collaboration 2024), deriving from the relative probability of two models, given the data. The frequentist metric is positive by construction, whereas for the Bayesian metric a negative value indicates a preference for the extended model compared to flat ΛCDM, and a positive value is a preference for flat ΛCDM.

For the Bayesian method, we use the interpretative scale given in table 1 of R. Trotta 2008 where $|\Delta \log \mathcal{Z}| < 1$ is inconclusive, $1 < |\Delta \log \mathcal{Z}| < 2.5$ is weak, $2.5 < |\Delta \log \mathcal{Z}| < 5.0$ is moderate and $5.0 < |\Delta \log \mathcal{Z}| < \infty$ is strong evidence for/against the model compared to flat ΛCDM.

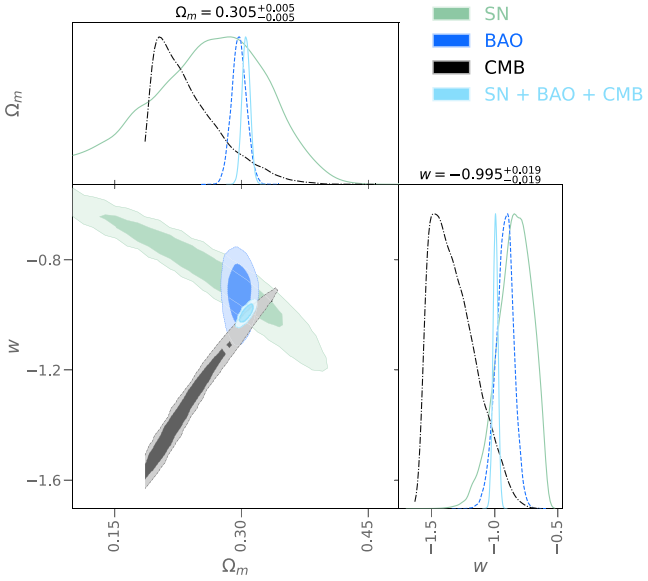

Figure 12. The Ω_m, w contours for flat wCDM. In green, we present SN-only, complemented by the CMB (black) and BAO (blue) constraints. The full combination of SN+BAO+CMB is in light blue. We include a maroon dashed line for $w = -1 = \Lambda$CDM.

For our full data combination, we find flat w_0w_aCDM is a better fit to the data by $\Delta\chi^2 = -13.5$ versus flat ΛCDM, which is a frequentist significance of 3.2σ. However, $\Delta \log \mathcal{Z} = -1.7$, a level which indicates a weak preference for evolving dark energy at odds of 5 : 1. In this context, there is not a strong evidential basis with the available data to conclude that dark energy evolves.

At first sight, it may appear that the frequentist 3.2σ and Bayesian 5 : 1 model odds are contradictory; we stress that with generally accepted 5σ threshold for rejection of the null hypothesis (here flat ΛCDM), they are consistent in their message. We discuss this further in Section 11.4.

It is clear from Table 10 that the full combination of data is required to show any Bayesian preference for evolving dark energy. We have also tested the BAO+CMB combination, also finding the evidence for flat w_0w_aCDM is weak. Notably, the SN+CMB combination shows a moderate preference for flat ΛCDM compared to flat w_0w_aCDM. Neither flat wCDM nor ΛCDM is favoured by any data combination.

Table 11 shows a summary of the results, visualized in Fig. 14.

11 DISCUSSION AND CONCLUSIONS

11.1 Comparison to DESI DR2

We benchmark our analysis choices by combining the original DES-SN5YR data set (as used in DESI Collaboration 2025) with BAO, but with our updated CMB data now including ACT and SPT (which were not available to DESI at their time of writing, but see C. Garcia-Quintero et al. 2025 for a discussion of the addition of ACT). We find a frequentist 4.0σ ($\Delta\chi^2 = -19.2$) compared to 4.2σ ($\Delta\chi^2 = -21.0$) in DESI DR2 (DESI Collaboration 2025 does not quote Bayesian evidences). The alignment is in part coincidental as the CMB likelihoods differ, and this is discussed in Section 11.4. We have also made use of the NAUTILUS sampler in Cosmosis rather than Cobaya MCMC sampler, but since our chains are well converged we expect this to be a minor effect.

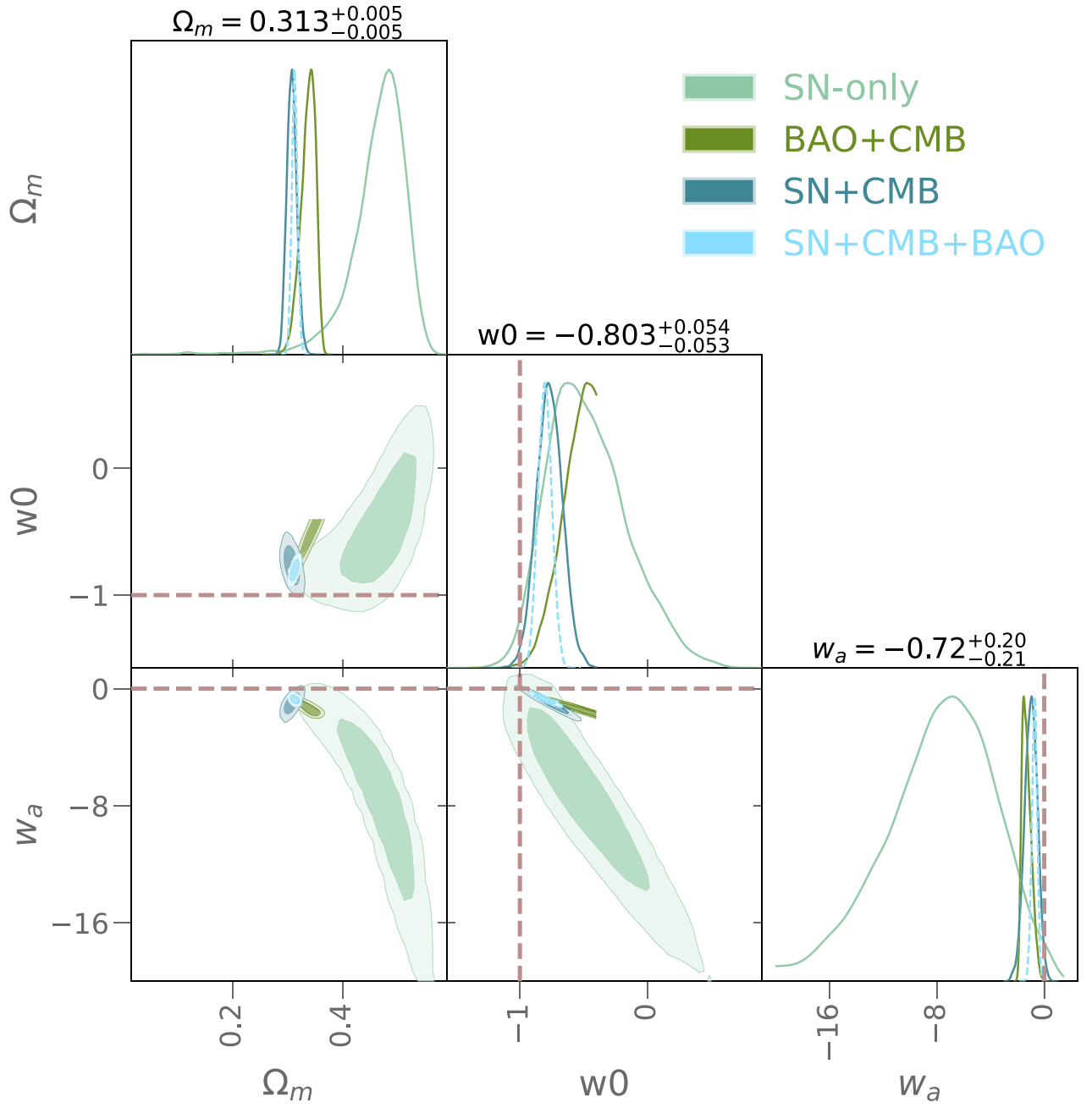

Figure 13. The cosmological contours for w_0w_aCDM cosmology. We show SN-only in light green, SN+CMB in blue, and SN+CMB+BAO in light blue. Our combined external probes, BAO+CMB, is shown in olive. We include light maroon dashed lines for $w = -1 = \Lambda$CDM.

Therefore, our results for DES-SN5YR are consistent with DESI Collaboration (2025) within the bounds of our differing choices.

11.2 The evidence for spatial flatness

It is well known that *Planck* DR3 data prefers a non-spatially flat Universe at over 2σ preference, however once low-redshift lensing, PANTHEON+ supernovae or BAO data from SDSS is included the preference disappears (see section 7.3 in Planck Collaboration VI 2020; G. Efstathiou & S. Gratton 2020). Interestingly, the over 2σ preference is restored when the CMB is combined with DESI DR2 BAO data (tables V and VI of DESI Collaboration 2025). As noted by S.-F. Chen & M. Zaldarriaga (2025), a non-spatially flat model provides a viable alternative to evolving dark energy when considering solely this data combination. For our data combination of SN+BAO+CMB, we find $\Omega_k = 0.0026 \pm 0.0011$, apparently also indicating a small non-zero spatial curvature.

However, we note the data combination of SN+CMB has $\Omega_k = -0.0063 \pm 0.0037$ (recall our CMB combination includes lensing data from *Planck*, ACT, and SPT) whereas for BAO+CMB it is $\Omega_k = 0.0025 \pm 0.0011$. The positive non-zero Ω_k for BAO+CMB appears to be driven by DESI DR2 favouring a lower Ω_m than the CMB, which drives a slight internal tension with SN Ia in ΛCDM. This is borne out in the SN+BAO+CMB combination, as the ΛCDM model is weakly disfavoured relative to flat-ΛCDM and moderately disfavoured relative to flat-w_0w_aCDM.

Table 10. Results for our different cosmological models, sorted into sections of different combinations of probes. We present the medians of the marginalized posterior with 68.27 per cent integrated uncertainties.

Ω_m	H_0	Ω_k	w_0	w_a	χ^2	$\log \mathcal{Z}$
DES-Dovekie (SN-only)						
Flat-ΛCDM	0.330 ± 0.015	–	–	–	–	1640.3	−822.5
ΛCDM	0.279 ± 0.057	–	0.14 ± 0.15	–	–	1639.5	−822.5
Flat-wCDM	$0.263^{+0.064}_{-0.078}$	–	–	$-0.838^{+0.130}_{-0.142}$	–	1639.0	−823.8
Flat-w_0w_aCDM	$0.473^{+0.035}_{-0.050}$	–	–	$-0.497^{+0.348}_{-0.267}$	$-7.46^{+3.60}_{-4.48}$	1634.2	−823.4
DES-Dovekie + CMB						
Flat-ΛCDM	0.317 ± 0.005	67.29 ± 0.34	–	–	–	2224.1	−1144.4
ΛCDM	0.335 ± 0.012	65.04 ± 1.24	$-0.0063 \pm +0.0037$	–	–	2219.9	−1145.4
Flat-wCDM	0.322 ± 0.008	66.70 ± 0.71	–	-0.978 ± 0.024	–	2223.1	−1147.7
Flat-w_0w_aCDM	0.308 ± 0.009	68.11 ± 0.89	–	-0.769 ± 0.100	-0.98 ± 0.48	2219.5	−1147.0
DES-Dovekie + BAO						
Flat-ΛCDM	0.306 ± 0.008	–	–	–	–	1654.5	−833.2
ΛCDM	0.293 ± 0.011	–	$0.054^{+0.033}_{-0.036}$	–	–	1652.4	−833.3
Flat-wCDM	0.297 ± 0.008	–	–	$-0.909^{+0.035}_{-0.037}$	–	1648.6	−833.5
Flat-w_0w_aCDM	$0.313^{+0.013}_{-0.016}$	–	–	$-0.843^{+0.071}_{-0.065}$	-0.53 ± 0.44	1647.2	−834.3
DES-Dovekie + CMB + BAO						
Flat-ΛCDM	0.304 ± 0.003	68.14 ± 0.23	–	–	–	2244.0	−1155.6
ΛCDM	0.305 ± 0.003	68.57 ± 0.30	0.0026 ± 0.0011	–	–	2238.4	−1156.7
Flat-wCDM	0.305 ± 0.005	68.02 ± 0.53	–	-0.995 ± 0.019	–	2244.5	−1159.6
Flat-w_0w_aCDM	0.313 ± 0.005	67.47 ± 0.55	–	-0.803 ± 0.054	-0.72 ± 0.21	2230.5	−1153.9

Table 11. The model preference metrics for our most constraining data combination, DES-Dovekie + CMB + BAO compared to flat ΛCDM. We provide the conversion of the $\Delta\chi^2_{\rm ML}$ into equivalent σ using Wilk's theorem and equation (10). The logarithm of the Bayes ratio is interpreted using an adaptation of the Jeffreys scale, given in table 1 of R. Trotta (2008), where $|\Delta \log \mathcal{Z}| \in (0, 1), (1, 2.5), (2.5, 5.0), (5.0, \infty)$ is inconclusive, weak, moderate, and strong evidences, respectively. A positive sign indicates the model is not preferred compared to flat ΛCDM, and a negative sign means it is preferred.

Model	$\Delta\chi^2_{\rm ML}$	σ	$\Delta \log \mathcal{Z}$	Bayesian model preference
Open ΛCDM	−5.6	2.3σ	+1.1	Weakly not preferred
Flat wCDM	0.0	0.0σ	+4.0	Moderately not preferred
Flat w_0w_aCDM	−13.5	$3.2\boldsymbol{\sigma}$	−1.7	Weakly preferred

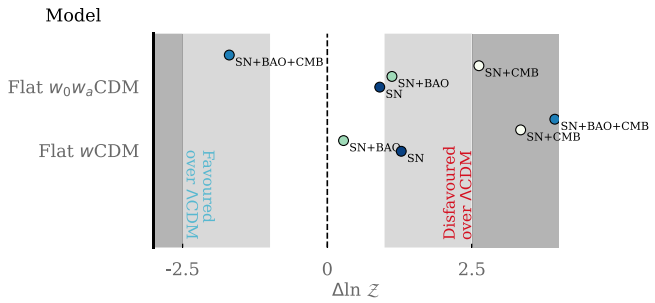

Figure 14. Model preference in terms of the log of the Bayes ratio, $\Delta \log \mathcal{Z}$.

Therefore, we conclude there is no evidence for non-zero spatial curvature arising from DES-Dovekie, DESI DR2, and CMB data.

11.3 The *Hubble* constant

The tension between the *Hubble* constant as measured from the local distance ladder, and as fit by a full redshift range of cosmological data remains an enduring mystery. For the CMB, Planck Collaboration VI (2020) reported $H_0 = 67.36 \pm 0.54$ km s^{-1} Mpc^{-1}, ACT reports 66.11 ± 0.79 km s^{-1} Mpc^{-1} (T. Louis et al. 2025), and SPT-3G gave $H_0 = 66.66 \pm 0.60$ km s^{-1} Mpc^{-1} (E. Camphuis et al. 2025). For the local distance ladder, recent results include $H_0 = 73.29 \pm 0.90$ km s^{-1} Mpc^{-1} (Y. S. Murakami et al. 2023) and $H_0 = 70.39 \pm 1.94$ km sec^{-1} Mpc^{-1} (W. L. Freedman et al. 2025), with large differences in the estimation of systematics. Improved photometry from the *James Webb Space Telescope* has not revealed any errors with earlier estimates due to lower resolution *HST* photometry (see e.g. A. G. Riess et al. 2025), and differences in local distance ladder may be traced to sample differences (A. G. Riess et al. 2024). Alternative probes have not matured as quickly as previously anticipated to provide an arbiter between these two clusters of results that is convincingly free of systematics (for a review, see e.g. P. Shah, P. Lemos & O. Lahav 2021).

Of course, BAO and SN Ia by themselves do not constrain H_0 as only relative observations are taken. The CMB constrains H_0 through the detailed shape of its power spectrum, which constrains the matter, baryon and photon densities prior to recombination, and hence the absolute scale of the temperature fluctuations (at least, in models without exotic additional physics pre-recombination). Combined with the angular size, the distance to the surface of last scattering is well constrained. Given a model for the subsequent evolution (by using the matter density and dark energy evolution as constrained by the CMB and low-redshift data, and again assuming no further exotic physics), H_0 is constrained (for a review, see e.g. P. Lemos & P. Shah 2024).

In flat-ΛCDM, our constraint of $H_0 = 68.14 \pm 0.25$ km s^{-1} Mpc^{-1} is discrepant from Y. S. Murakami et al. (2023) at the level of 5.5σ. However, the errors are primarily driven by the CMB and BAO data rather than SN Ia for this model. It is modestly

tighter than $H_0 = 67.24 \pm 0.35$ km s^{-1} Mpc^{-1} quoted in table I of E. Camphuis et al. (2025) for their CMB-SPA combination, due to the inclusion of BAO data. Similarly, is also modestly tighter than 68.17 ± 0.28 km s^{-1} Mpc^{-1} quoted in table V of DESI Collaboration (2025) for their DESI+CMB combination, due to the inclusion of more CMB data.

Additional variation of H_0 is allowed in extended models of dark energy. The general trend when adding DESI DR2 data is for lower H_0 (as pointed out by A. Lewis & E. Chamberlain 2025) which works against the larger error bars in converting to a tension. For the extended model, it is notable that SN Ia data are helpful in constraining H_0. The CMB+BAO combination results in $64.88^{+1.52}_{-1.06}$ km s^{-1} Mpc^{-1}, whereas CMB+SN Ia has 68.11 ± 0.89 km s^{-1} Mpc^{-1}, a discrepancy of 1.8σ. Interestingly, our combined CMB+BAO+SN Ia constraint for flat-w_0w_aCDM is $H_0 = 67.47 \pm 0.55$ km s^{-1} Mpc^{-1} is within 0.2σ of the flat ΛCDM value for CMB data only.

Our combination of CMB+BAO+SN Ia represents an inverse distance ladder. In effect, the matter density of the Universe throughout cosmic time and the absolute size of the BAO are determined by the CMB (and the pre-CMB evolution is assumed to be free of exotic physics such as Early Dark Energy). The residual departure of SNe and BAO distances in the late Universe are small, and able to be captured within the framework of flat w_0w_aCDM (and more general evolution, as emphasized in K. Lodha et al. 2025). The question of whether dark energy evolves or not in the late Universe is unconnected with any potential resolution of the *Hubble* constant tension.

11.4 The evidence for evolving dark energy

In this paper, we have presented a re-analysis of the DES-SN5YR data with an updated filter recalibration, incorporating extra degrees of model freedom and more calibration data. The result of our re-analysis is that the evidence for flat w_0w_aCDM over flat ΛCDM is reduced by $\Delta \log \mathcal{Z}$ 3.5 compared to DES-SN5YR, which is enough to downgrade the preference for evolving dark energy from strong to weak.

As discussed previously, model preference can be assessed both in a frequentist or Bayesian framework. While a detailed review is beyond the scope of this paper, we should expect that differing choices be consistent in their message. We consider a frequentist 3.2σ to be consistent with our classification of the log Bayes ratio of -1.7 (model odds of 5:1) as weak evidence in favour of evolving dark energy, as it is generally accepted that 5σ is an appropriate threshold for a strong rejection of the null hypothesis that the Universe is flat ΛCDM. In a hypothetical scenario where SN+CMB+BAO data indeed indicated a frequentist preference of 5σ, we estimate the log Bayes ratio would be ~ -8, a level which would be indeed be classified as strong on our interpretative scale. While Bayesian evidence does depend on the choice of prior, within reasonable ranges of choices (that is, broadly consistent with other astrophysical and physical constraints, such as structure formation) this equivalence would not be materially affected.

In terms of the *Hubble* diagram, our change in preference for evolving dark energy can be attributed to the reduction in the relative dimness of low-redshift SNe, relative to mid-redshift SNe, as is apparent in Fig. 3. This in turn is driven by a change in the SNe light-curve fitting model SALT (which is trained on data from multiple surveys and hence multiple filters) and a change in the effective definition of the DES$-g$ band, from Dovekie restoring the original PS1$-g$ reference filter, as shown in fig. 14 in Dovekie. We emphasize that this change is driven solely by improvement to the data (in particular, the addition of DA white dwarfs as calibrator stars) and methodology used for filter recalibration, and corrections to the shape of the colour law. It is also consistent with previously reported systematics. Table 9 shows that our $\sigma(\text{phot})_{\text{syst}}$ uncertainties are well calibrated.

The preference for w_0w_aCDM cosmology is not driven by changes to the SNe alone. The influence of the choice of low-ℓ CMB likelihood on the preference for evolving dark energy has been noted in C. Garcia-Quintero et al. (2025) and N. Sailer et al. (2026). In general terms, $\Omega_{\rm m}$ determines the peak heights of the CMB power spectrum, but also so does the Thomson scattering of CMB photons by the charged intergalactic medium in the epoch post-reionization. This leads to a degeneracy between $\Omega_{\rm m}$ and the optical depth parameter τ, which is determined by the CMB polarization. Higher τ leads to a lower preference for evolving dark energy. We have tested the impact of different choices of CMB likelihood by successively removing SPT and ACT data, and replacing the low-ℓ`simall` likelihood with a τ-prior from the `Srol12` likelihood (J. M. Delouis et al. 2019, as is done in T. Louis et al. 2025). The choices all reduce our preference for evolving dark energy by between 0.2 to 0.7σ, or in Bayesian terms by up to $\delta \log \mathcal{Z} \sim 3.0$. Although we do not test specifically the combination used in DESI DR2, it is likely given the low optical depth noted for that choice in E. Rosenberg, S. Gratton & G. Efstathiou (2022) that the preference for evolving dark energy from that choice is at the upper end of the combinations we tested.

All told, our results place DES-Dovekie as intermediate in preference for evolving dark energy, in between PANTHEON+ and Union3 (which DESI Collaboration 2025 quotes as $\Delta\chi^2 = -10.7$ and -17.4 respectively), and consistent with both. Moreover, it should be emphasized that the three supernova data sets in common use: PANTHEON+, Union3, and DES-Dovekie are all consistent with each other, with differences between them at the $\lesssim 1\sigma$ level in terms of cosmological parameters. Approximately adjusting these numbers for our analysis choices, we estimate that a Bayes ratio for the PANTHEON+ data set would also show no evidence in favour of w_0w_aCDM, and Union3 would moderately prefer it, indicating that our conclusion that there is no strong preference for evolving dark energy is robust to other choices of SN Ia data.

11.5 Improvements over DES-SN5YR

This work is best understood as part of an ongoing effort within the SN Ia community to improve modelling and facilitate reanalysis of photometric data. This continues the trend of greater data volumes informing the modelling techniques, in turn leading to better understanding of systematics, that has been in progress over the last 25 yr.

It has been argued that the evidence for evolving dark energy reported in DESI Collaboration (2025) is a consequence of SNe systematics (G. Efstathiou 2024) or inconsistencies between cosmological parameters across probes (X. T. Tang et al. 2025). While the apparent inconsistency of SN Ia distances in common to different data sets was largely explained as the consequence of differing selection functions, scatter models, and mass calibration in M. Vincenzi et al. (2025), the question remains: how safe are SNe data?

Broadly, most supernovae systematics fall into the three categories of photometric calibration, foregrounds or astrophysical processes. Our paper addresses the first of these, and may be

regarded as a continuation of the investigation of M. Vincenzi et al. (2025).

During our re-creation of the DES-SN5YR data set, we discovered an outdated approximation used for the E. L. Fitzpatrick (1999) colour law. We also found that the systematic uncertainty for calibration had been underweighted (Section 5), and this was corrected here as well. Considering sequential changes from DES-SN5YR, the colour law corrected DES-SN5YR increases Ω_m by $\sim 1\sigma$, and then DES-Dovekie photometric recalibration decreases Ω_m by $\sim 2\sigma$. Although these changes are notable when considered in isolation, this neglects the correlation with the rest of the pipeline, and the change is less significant in extended models (Table 7).

The new calibration and updated SALT model do not cause any obvious changes to our observed distribution of SN Ia properties, save that of the DES c distribution, which is different at 2.8σ from DES-SN5YR. Investigating further, we find that this change in the DES c distribution is predicted when simulating with the DES-SN5YR simulation parameters, resulting in good agreement between our simulated and observed c distributions (Fig. 4). Therefore, the change in our observed colour is entirely explained by the change of SALT model.

It is a familiar refrain that the ~ 200 SNe low-redshift sample in DES-SN5YR (and earlier data sets) requires modernizing. Unfortunately, some of these older low-redshift samples, such as CfA3, contain spectral sequences that are believed essential for SALT training. Incorporating these spectral sequences involves cross-calibrating these older samples, thereby increasing the calibration systematic even in the case of single-telescope cosmology analyses (e.g. a DECam low-z sample+DES, or PS1+Foundation). Fully replacing these older samples will require either more complete knowledge of the impact of dropping these spectral sequences, or a sample that includes these sequences with a better-understood calibration path.

Given the change in the SALT model, calibration, and the F99 colour law, a natural question that arises is the necessity of recalibrating the scatter model by updating the DUST2DUST fitting code (B. Popovic et al. 2023) to use the exact F99 colour law. We find that the χ^2/ν changes by < 1 between the approximate and exact F99 colour laws, which we did not find sufficient to require a re-determination of the intrinsic SN Ia and dust parameters. When comparing the DUST2DUST metrics from the original SALT3.DES5YR (c, $\mu_{\rm res}$, $\sigma\mu_{\rm res}$), we find that the new data/simulation agreement is slightly worse than the original DES-SN5YR. This behaviour is not driven by any individual metric, but rather a general trend. Given recent improvements in our understanding of host-galaxy environs (S. González-Gaitán et al. 2021; L. Kelsey et al. 2023; M. Grayling et al. 2024; M. Ginolin et al. 2025), there is ample opportunity for future work to improve upon dust modelling. Upcoming low-redshift samples such as ATLAS (J. L. Tonry et al. 2018) or DEBASS (N. F. Sherman et al. 2025; M. Acevedo et al. 2026) in the near future, or the Zwicky Transient Facility (M. Rigault et al. 2025) and LS4 (A. A. Miller et al. 2025) present exciting opportunities for combination with DES-Dovekie.

The LSST-TiDES (C. Frohmaier et al. 2025) survey is forecast to assemble a Hubble diagram of $\sim 140\,000$ SN Ia with spectroscopic redshifts (either directly from the SN Ia spectral sequence, or the host galaxy). On current systematic errors therefore, this data would be systematic-limited. Fortunately there are grounds for optimism that systematics will keep pace, with the above mentioned improvements in low-z data, plus LSST-TiDES data itself. Low-z SN Ia are useful not only to control systematics: the Universe starts to accelerate at $z \sim 0.7$, and becomes dark energy dominated at $z \sim 0.3$. While high-z SN Ia are important to establish consistency of the matter density between the CMB, BAO, and SN Ia, it is in the redshift range $z < 0.5$ that we obtain most information about potential dark energy evolution.

In summary, DES supernovae remain the best-characterized high-redshift sample before LSST. Further improvements to the understanding of environmental factors and their impact on cosmology will doubtless be achieved; but DES-Dovekie demonstrates that the source of the current ΛCDM tension is very unlikely to arise solely from photometric cross-calibration. As such, we recommend the distances in this paper supersede the original DES-SN5YR distances.

AUTHOR CONTRIBUTIONS

BP performed the analysis, drafted the manuscript, and determined the visual language of the work. PS contributed to the analysis – cosmology fits and statistical tests for cosmological preferences in particular – and manuscript preparation. WDK aided in the analysis, unblinding, and writing of the paper. RK performed continuation and upgrades of SNANA and general writing/issue-solving aid. TD, provided detailed feedback on the analysis, and along with DS, served as internal reviewer. AG provided writing and analysis guidance. MV provided discussion on cosmological results and pipeline implementation. PW, RC, and EC provided help to generate simulations. JF, LG, JL, AM, and BS provided comments on the manuscript. The remaining authors have made contributions to this paper that include, but are not limited to, the construction of DECam and other aspects of collecting the data; data processing and calibration; developing broadly used methods, codes, and simulations; running the pipelines and validation tests; and promoting the science analysis.

ACKNOWLEDGEMENTS

This work was completed in part with resources provided by the University of Chicago's Research Computing Center. This project has received funding from the European Union's Horizon Europe research and innovation programme under the Marie Skłodowska-Curie grant agreement no. 101205780. This work has been supported by the research project grant 'Understanding the Dynamic Universe' funded by the Knut and Alice Wallenberg Foundation under Dnr KAW 2018.0067 and the *Vetenskapsrådet*, the Swedish Research Council, project 2020–03444.

BP acknowledges you, gentle reader. PW acknowledges support from the Science and Technology Facilities Council (STFC) grant ST/Z510269/1. TD acknowledges support from the Australian Research Council through the ARC Centre of Excellence for Gravitational Wave Discovery (OzGrav), CE230100016. LK acknowledges support for an Early Career Fellowship from the Leverhulme Trust through grant ECF-2024-054 and the Isaac Newton Trust through grant 24.08(w). AM is supported by the Australian Research Council DE230100055. PA acknowledges that parts of this research was carried out on the traditional lands of the Ngunnawal people. We pay our respects to their elders past, present, and emerging. LG acknowledges financial support from AGAUR, CSIC, MCIN, and AEI 10.13039/501100011033 under projects PID2023-151307NB-I00, PIE 20215AT016, CEX2020-001058-M, ILINK23001, COOPB2304, and 2021-SGR-01270.

DATA AVAILABILITY

Data used in this article are publicly available with the DES-SN5YR data release from B. O. Sánchez et al. (2024), hosted at https://github.com/des-science/DES-SN5YR.

The analysis files used for this work are included with the public SNANA install on Zenodo, and the data products of this work are available publicly at https://github.com/des-science/DES-SN5YR

REFERENCES

Abbott T. M. C. et al., 2019, ApJ, 872, L30
Abbott T. M. C. et al., 2024, Phys. Rev. D, 110, 063515
Acevedo M. et al., 2026, ApJ, 996, 7
Alam S. et al., 2017, MNRAS, 470, 2617
Alam S. et al., 2021, Phys. Rev. D, 103, 083533
Axelrod T. et al., 2023, ApJ, 951, 78
Babusiaux C. et al., 2023, A&A, 674, A32
Balkenhol L., Trendafilova C., Benabed K., Galli S., 2024, A&A, 686, A10
Betoule M. et al., 2014, A&A, 568, A22
Bianchi L., Shiao B., Thilker D., 2017, ApJS, 230, 24
Bohlin R. C., Gordon K. D., Tremblay P.-E., 2014, PASP, 126, 711
Boyd B. M. et al., 2025, MNRAS, 540, 385
Brout D., Scolnic D., 2021, ApJ, 909, 26
Brout D. et al., 2019, ApJ, 874, 150
Brout D. et al., 2022a, ApJ, 938, 111
Brout D. et al., 2022b, ApJ, 938, 110
Calcino J., Davis T., 2017, J. Cosmol. Astropart. Phys., 2017, 038
Camilleri R. et al., 2024, MNRAS, 533, 2615
Camphuis E. et al., 2025, preprint (arXiv:2506.20707)
Cardelli J. A., Clayton G. C., Mathis J. S., 1989, ApJ, 345, 245
Carr A., Davis T. M., Scolnic D., Said K., Brout D., Peterson E. R., Kessler R., 2022, PASA 39, e046
Carron J., Mirmelstein M., Lewis A., 2022, J. Cosmol. Astropart. Phys., 2022, 039
Chen S.-F., Zaldarriaga M., 2025, J. Cosmol. Astropart. Phys., 2025, 014
Chevallier M., Polarski D., 2001, Int. J. Mod. Phys. D, 10, 213
Childress M. J. et al., 2017, MNRAS, 472, 273
DES Collaboration, 2024, ApJ, 973, L14
DES Collaboration, 2026a, preprint (arXiv:2602.10065)
DES Collaboration, 2026b, Phys. Rev. D, 113, 063530
DESI Collaboration, 2025, Phys. Rev. D, 112, 083515
Dark Energy Survey Collaboration, 2016, MNRAS, 460, 1270
Delouis J. M., Pagano L., Mottet S., Puget J. L., Vibert L., 2019, A&A, 629, A38
Dhawan S., Popovic B., Goobar A., 2025, MNRAS, 540, 1626
Efstathiou G., 2024, MNRAS, 538, 875
Efstathiou G., Gratton S., 2020, MNRAS, 496, L91
Fioc M., Rocca-Volmerange B., 1999, preprint (arXiv:astro-ph/9912179)
Fitzpatrick E. L., 1999, PASP, 111, 63
Flaugher B. et al., 2015, AJ, 150, 150
Foley R. J. et al., 2018, MNRAS, 475, 193
Freedman W. L., Madore B. F., Hoyt T. J., Jang I. S., Lee A. J., Owens K. A., 2025, ApJ, 985, 203
Frohmaier C. et al., 2025, ApJ, 992, 158
Gaia Collaboration, 2016, A&A, 595, A1
Gaia Collaboration, 2023, A&A, 674, A1
Garcia-Quintero C. et al., 2025, Phys. Rev. D, 112, 083529
Ginolin M. et al., 2025, A&A, 694, A4
González-Gaitán S., de Jaeger T., Galbany L., Mourão A., Paulino-Afonso A., Filippenko A. V., 2021, MNRAS, 508, 4656
Grayling M., Thorp S., Mandel K. S., Dhawan S., Uzsoy A. S. M., Boyd B. M., Hayes E. E., Ward S. M., 2024, MNRAS, 531, 953
Gupta R. R. et al., 2016, AJ, 152, 154
Guy J. et al., 2010, A&A, 523, A7
Handley W., Lemos P., 2019, Phys. Rev. D, 100, 023512
Hartley W. G. et al., 2022, MNRAS, 509, 3547
Hicken M. et al., 2009, ApJ, 700, 331
Hicken M. et al., 2012, ApJS, 200, 12
Hinton S., Brout D., 2020, J. Open Source Softw., 5, 2122
Hlozek R. et al., 2012, ApJ, 752, 79
Jones D. O. et al., 2017, ApJ, 843, 6
Jones D. O. et al., 2018, ApJ, 857, 51
Kelly P. L., Hicken M., Burke D. L., Mandel K. S., Kirshner R. P., 2010, ApJ, 715, 743
Kelsey L. et al., 2023, MNRAS, 519, 3046
Kenworthy W. D. et al., 2021, ApJ, 923, 265
Kessler R., Scolnic D., 2017, ApJ, 836, 56
Kessler R. et al., 2009, PASP, 121, 1028
Kessler R. et al., 2015, AJ, 150, 172
Kessler R. et al., 2019, PASP, 131, 094501
Knights M., Bassett B. A., Varughese M., Hlozek R., Kunz M., Smith M., Newling J., 2013, J. Cosmol. Astropart. Phys., 2013, 039
Krisciunas K. et al., 2017, AJ, 154, 211
Kroupa P., 2001, MNRAS, 322, 231
Kunz M., Bassett B. A., Hlozek R. A., 2007, Phys. Rev. D, 75, 103508
Lampeitl H. et al., 2010, ApJ, 722, 566
Lange J. U., 2023, MNRAS, 525, 3181
Lasker J. et al., 2019, MNRAS, 485, 5329
Le Borgne D., Rocca-Volmerange B., 2002, A&A, 386, 446
Lee J. et al., 2023, AJ, 165, 222
Lemos P., Lewis A., 2023, Phys. Rev. D, 107, 103505
Lemos P., Shah P., 2024, in Di Valentino E., Dillon Brout, eds, The Hubble Constant Tension. p. 295
Lewis A., Chamberlain E., 2025, J. Cosmol. Astropart. Phys., 2025, 065
Lidman C. et al., 2020, MNRAS, 496, 19
Lilow R., Nusser A., 2021, MNRAS, 507, 1557
Linder E. V., 2003, Phys. Rev. Lett., 90, 091301
Linder E. V., 2007, preprint (arXiv:0708.0024)
Lodha K. et al., 2025, Phys. Rev. D, 112, 083511
Louis T. et al., 2025, J. Cosmol. Astropart. Phys., 2025, 062
Madhavacheril M. S. et al., 2024, ApJ, 962, 113
Mandel K. S., Thorp S., Narayan G., Friedman A. S., Avelino A., 2022, MNRAS, 510, 3939
Miller A. A. et al., 2025, PASP, 137, 094204
Möller A., de Boissière T., 2020, MNRAS, 491, 4277
Möller A. et al., 2022, MNRAS, 514, 5159
Möller A. et al., 2024, MNRAS, 533, 2073
Murakami Y. S. et al., 2023, J. Cosmol. Astropart. Phys., 2023, 046
Naess S. et al., 2025, J. Cosmol. Astropart. Phys., 2025, 061
Narayan G. et al., 2019, ApJS, 241, 20
Nicolas N. et al., 2021, A&A, 649, A74
Pan Z. et al., 2023, Phys. Rev. D, 108, 122005
Perlmutter S. et al., 1999, ApJ, 517, 565
Perrett K. et al., 2010, AJ, 140, 518
Peterson E. R. et al., 2022, ApJ, 938, 112
Planck Collaboration V, 2020, A&A, 641, A5
Planck Collaboration VI, 2020, A&A, 641, A6
Popovic B., Brout D., Kessler R., Scolnic D., Lu L., 2021, ApJ, 913, 49
Popovic B. et al., 2024, MNRAS, 529, 2100
Popovic B., Brout D., Kessler R., Scolnic D., 2023, ApJ, 945, 84
Popovic B. et al., 2025, preprint (arXiv:2506.05471)
Prince H., Dunkley J., 2019, Phys. Rev. D, 100, 083502
Qu F. J. et al., 2024, ApJ, 962, 112
Qu H., Sako M., Möller A., Doux C., 2021, AJ, 162, 67
Qu H. et al., 2024, ApJ, 964, 134
Riess A. G. et al., 1998, AJ, 116, 1009
Riess A. G. et al., 2024, ApJ, 977, 120
Riess A. G. et al., 2025, ApJ, 992, L34
Rigault M. et al., 2025, A&A, 694, A1
Rosenberg E., Gratton S., Efstathiou G., 2022, MNRAS, 517, 4620
Rubin D. et al., 2025, ApJ, 986, 231
Sailer N., Farren G. S., Ferraro S., White M., 2026, Phys. Rev. Lett., 136, 081002

Sánchez B. O. et al., 2022, ApJ, 934, 96
Sánchez B. O. et al., 2024, ApJ, 975, 5
Schlafly E. F., Finkbeiner D. P., 2011, ApJ, 737, 103
Scolnic D. et al., 2018, ApJ, 852, L3
Shah P., Lemos P., Lahav O., 2021, A&AR, 29, 9
Sherman N. F. et al., 2025, preprint (arXiv:2508.10878)
Sivia D., Skilling J., 2006, Data Analysis – A Bayesian Tutorial. Oxford Univ. Press
Smith G. A. et al., 2004, in Moorwood A. F. M., Iye M., eds, Proc. SPIE Conf. Ser. Vol. 5492, Ground-based Instrumentation for Astronomy. SPIE, Bellingham, p. 410
Smith M. et al., 2020, MNRAS, 494, 4426
Sullivan M. et al., 2006, ApJ, 648, 868
Sullivan M. et al., 2010, MNRAS, 406, 782
Tang X. T., Brout D., Karwal T., Chang C., Miranda V., Vincenzi M., 2025, ApJ, 983, L27
Taylor G. et al., 2023, MNRAS, 520, 5209
Thorp S., Mandel K. S., Jones D. O., Kirshner R. P., Challis P. M., 2024, MNRAS, 530, 4016
Tonry J. L. et al., 2012, ApJ, 750, 99
Tonry J. L. et al., 2018, PASP, 130, 064505
Tripp R., 1998, A&A, 331, 815
Trotta R., 2008, Contemp. Phys., 49, 71
Vincenzi M., Sullivan M., Firth R. E., Gutiérrez C. P., Frohmaier C., Smith M., Angus C., Nichol R. C., 2019, MNRAS, 489, 5802
Vincenzi M. et al., 2023, MNRAS, 518, 1106
Vincenzi M. et al., 2024, ApJ, 975, 86
Vincenzi M. et al., 2025, MNRAS, 541, 2585
Wilks S., 1938, Annals Math. Statist., 9
Wiseman P. et al., 2020, MNRAS, 495, 4040
Wiseman P. et al., 2022, MNRAS, 515, 4587
Yuan F. et al., 2015, MNRAS, 452, 3047
Zuntz J. et al., 2015, Astron. Comput., 12, 45

APPENDIX A: FITZPATRICK 99 CHANGES

Since approximately 2013, SNANA had used a polynomial expansion of the E. L. Fitzpatrick (1999) colour law, centred at $R_v = 3.1$. In the process of integrating BAYESN (K. S. Mandel et al. 2022; M. Grayling et al. 2024; S. Thorp et al. 2024) into SNANA, this approximation was discovered by comparing the original BAYESN code with the SNANA development version. The SNANA polynomial was replaced with the full F99 colour law by Dr Stephen Thorp in early 2025. In Fig. A1, we show the Δmag as a function of wavelength between the previous approximation and the exact colour law, for various R_V values.

For the $R_V \geq 2$ regime, these changes are close to negligible within the SALT model range (2000–11 000 Å). However, DES-SN5YR, in addition to AMALGAME (B. Popovic et al. 2024) and PANTHEON+, use simulated supernovae drawn from a Gaussian distribution that spans approximately $1.4 < R_V \leq 4$, necessitating a regeneration of the bias correction simulations. The impact of this change is shown in Appendix B.

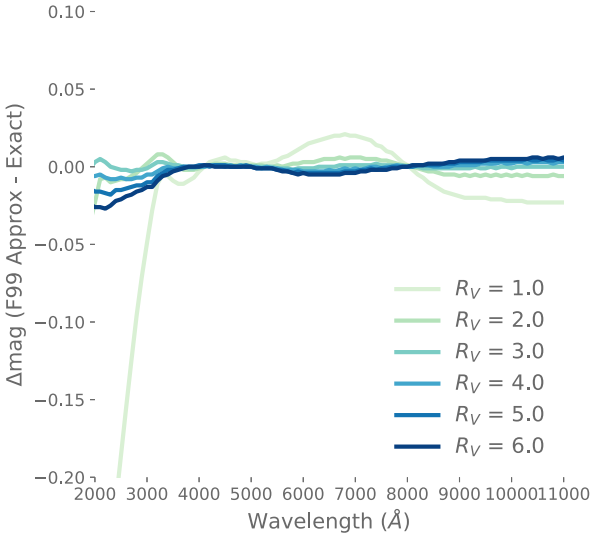

Figure A1. The magnitude difference between the former F99 approximation and the exact F99 colour law, as a function of wavelength. We show this for several selected R_V values, from $R_V = 1$ to 6.

APPENDIX B: COSMOLOGY WITH F99 FIX

Figs B1 and B2 show our posteriors for flat ΛCDM and w_0w_aCDM cosmologies, after updating the M. Vincenzi et al. (2024) pipeline to include the fix to the F99 colour law, but before the Dovekie re-calibration is done. In ΛCDM we find $\Omega_m = 0.369 \pm 0.017$, a level which is 2.8σ discrepant with the *Planck* CMB. In w_0w_aCDM we find $w_0, w_a = -0.74 \pm 0.06, -0.80^{+0.23}_{-0.24}$, increasing the inconsistency of the data with ΛCDM by 0.3σ.

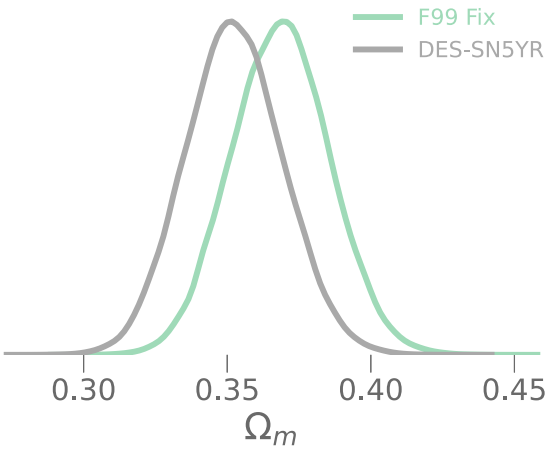

Figure B1. Ω_m posteriors in flat-ΛCDM for the original DES-SN5YR (grey) and the F99 colour law fix (light green). The F99 fix moves the matter density before re-calibration to be relatively higher compared to the CMB by $\sim 1\sigma$.

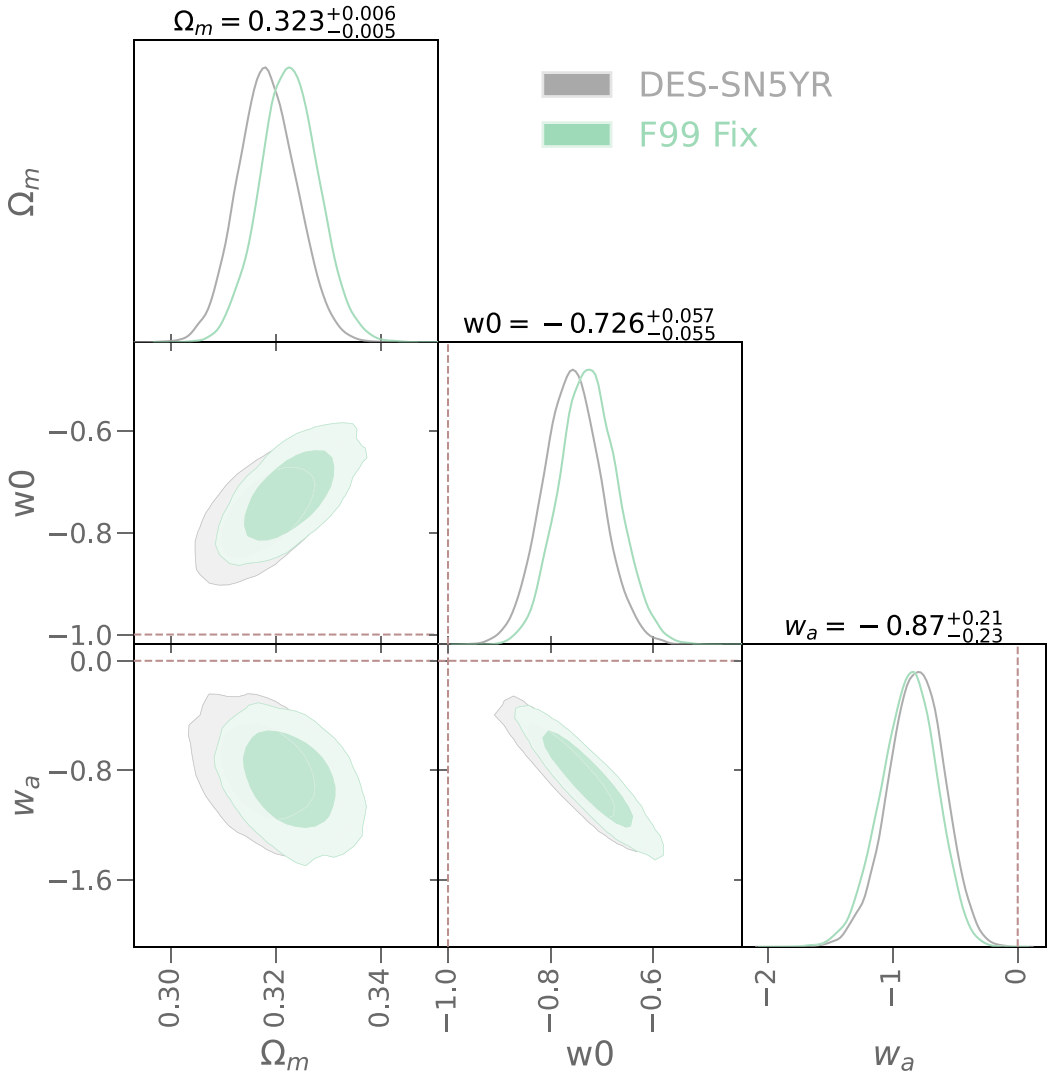

Figure B2. Ω_m, w_0, and w_a posteriors, from the combined SN+BAO+CMB sample for DES-SN5YR (grey) and the F99 colour law fix (light green). The F99 fix increases the discrepancy with ΛCDM (note this is before recalibration).

APPENDIX C: COMPARISON TO DES-SN5YR

In this section, we highlight the changes in cosmology results between DES-SN5YR and DES-Dovekie. Table C1 shows the difference in cosmological results for SN-only and SN+CMB+BAO, the most instructive and most interesting combination of probes respectively. Fig. C1 shows the SN-only flat ΛCDM posterior for

Table C1. A selection of the DES-Dovekie–DES-SN5YR changes in cosmology.

Model	$\Delta\Omega_m$	Δw	Δw_a
SN-only flat ΛCDM	−0.022	–	–
SN-only ΛCDM	−0.020	–	–
SN-only flat wCDM	−0.007	−0.031	–
SN-only flat w_0w_aCDM	−0.023	−0.138	1.47
SN+CMB+BAO flat ΛCDM	−0.001	–	–
SN+CMB+BAO ΛCDM	−0.001	–	–
SN+CMB+BAO flat wCDM	−0.004	−0.015	–
SN+CMB+BAO flat w_0w_aCDM	−0.006	−0.052	0.130

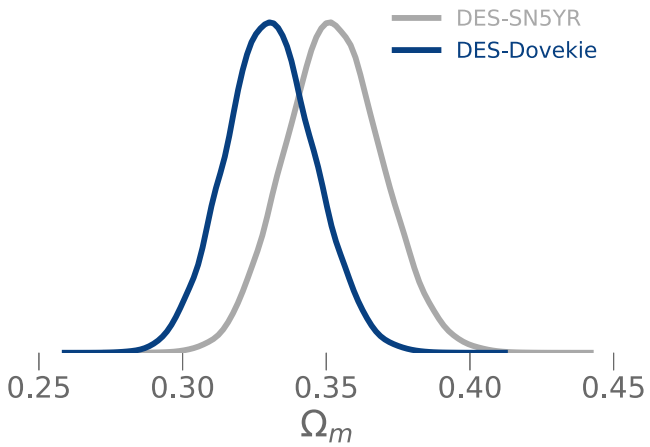

Figure C1. Ω_m posteriors for flat ΛCDM for the original DES-SN5YR (grey) and DES-Dovekie (dark blue).

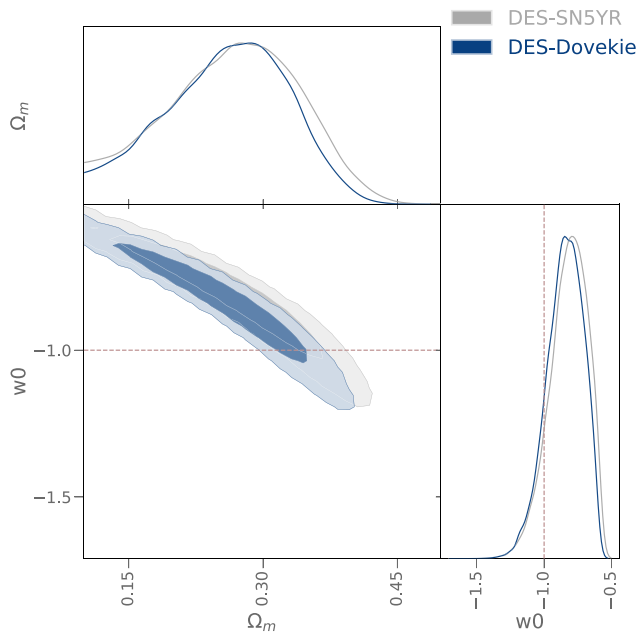

Figure C2. Comparison between DES-SN5YR and DES-Dovekie contours for the flat-wCDM model. In grey, we present the DES-SN5YR contours, and the DES-Dovekie contours in dark blue. We provide a light maroon dashed line at $w = -1$, the cosmological constant.

DES-Dovekie and DES-SN5YR, and Fig. C2 shows the same, but for wCDM.

In all cases, DES-Dovekie finds a lower Ω_m, resulting in greater consistency between SN, CMB, and BAO. For w_0 and w_a, DES-Dovekie prefers w_0 closer to -1 and w_a slightly closer to zero. The shifts in wCDM are within our systematic uncertainty for calibration as in Table 8, a qualitative 0.5σ. Fig. C3 compares the SN-only constraints for DES-SN5YR and DES-Dovekie.

DES-Dovekie parameter uncertainties are lower compared to DES-SN5YR, as a result of the greater internal consistency of the data. $\sigma(\Omega_m)$ is 10 per cent lower in flat ΛCDM, flat wCDM, and flat w_0w_aCDM, as is $\sigma(w_0)$ and $\sigma(w_a)$ in extended dark energy models.

Finally, we note that the d.o.f. of DES-Dovekie are 1684, slightly lower than DES5YR. This value is obtained by summing the BEAMS probability from BBC.

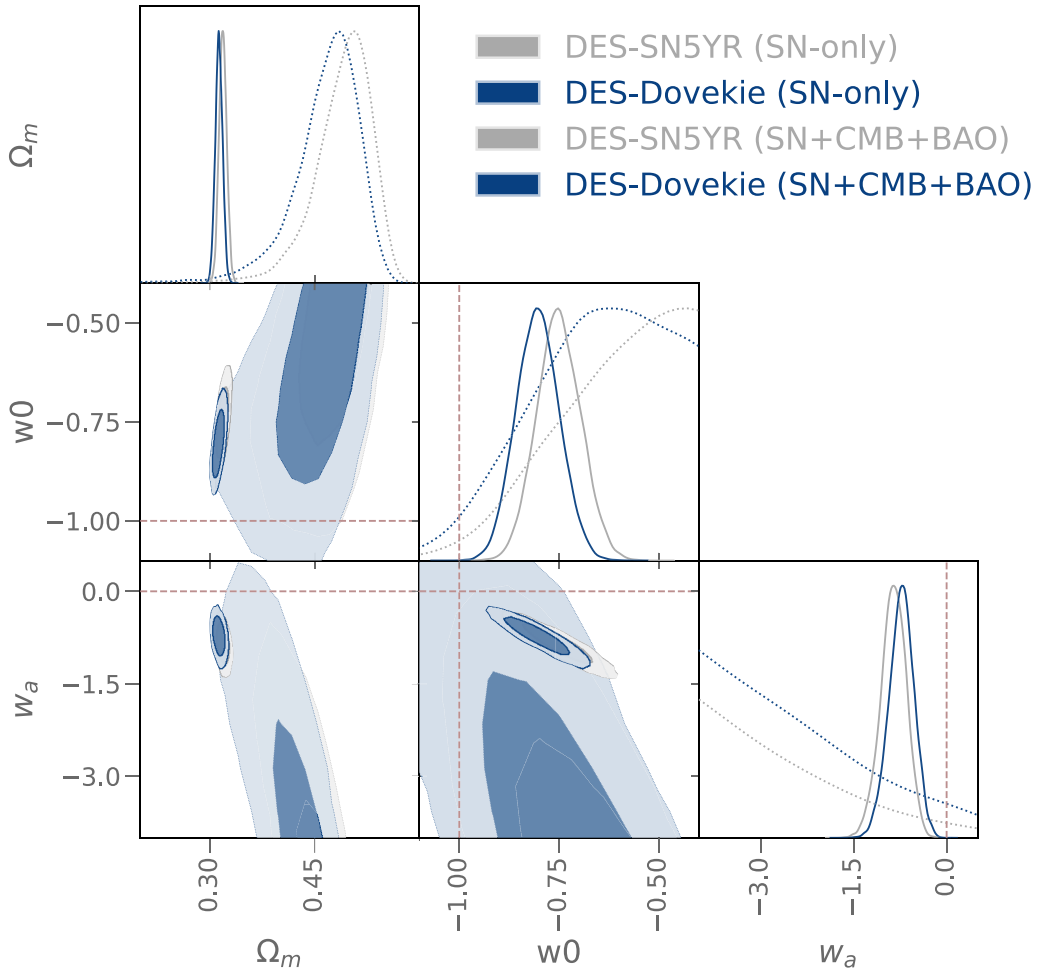

Figure C3. Ω_m, w_0, and w_a posteriors for SN+CMB+BAO with SN Ia as DES-SN5YR (grey) and DES-Dovekie (dark blue). We present the SN-only posteriors for each in high transparency.

[1]*Universite Claude Bernard Lyon 1, CNRS, IP2I Lyon/IN2P3, IMR 5822, F-69622 Villeurbanne, France*
[2]*School of Physics and Astronomy, University of Southampton, Southampton SO17 1BJ, UK*
[3]*Department of Physics & Astronomy, University College London, Gower Street, London WC1E 6BT, UK*
[4]*The Oskar Klein Centre, Department of Physics, Stockholm University, SE-106 91 Stockholm, Sweden*
[5]*Department of Astronomy and Astrophysics, University of Chicago, Chicago, IL 60637, USA*
[6]*Kavli Institute for Cosmological Physics, University of Chicago, Chicago, IL 60637, USA*
[7]*School of Mathematics and Physics, University of Queensland, Brisbane, QLD 4072, Australia*
[8]*Department of Physics, Duke University, Durham, NC 27708, USA*
[9]*Department of Physics, University of Oxford, Denys Wilkinson Building, Keble Road, Oxford OX1 3RH, UK*
[10]*Department of Physics, Duke University, Durham, NC 27708, USA*
[11]*The Research School of Astronomy and Astrophysics, Australian National University, Canberra, ACT 2601, Australia*
[12]*Institute of Astronomy and Kavli Institute for Cosmology, Madingley Road, Cambridge CB3 0HA, UK*
[13]*Center for Astrophysics | Harvard & Smithsonian, 60 Garden Street, Cambridge, MA 02138, USA*
[14]*Fermi National Accelerator Laboratory (FNAL), PO Box 500, Batavia, IL 60510, USA*
[15]*Institute of Space Sciences (ICE, CSIC), Campus UAB, Carrer de Can Magrans, s/n, E-08193 Barcelona, Spain*
[16]*Institut d'Estudis Espacials de Catalunya (IEEC), E-08034 Barcelona, Spain*
[17]*Department of Physics and Astronomy, Baylor University, One Bear Place 97316, Waco, TX 76798-7316, USA*
[18]*Université Grenoble Alpes, CNRS, LPSC-IN2P3, F-38000 Grenoble, France*
[19]*Department of Physics and Astronomy, University of Pennsylvania, Philadelphia, PA 19104, USA*
[20]*Centre for Astrophysics & Supercomputing, Swinburne University of Technology, Swinburne, VIC 3122, Australia*
[21]*Department of Physics, Lancaster University, Lancs LA1 4YB, UK*
[22]*Institute of Space Sciences (ICE, CSIC), Campus UAB, Carrer de Can Magrans, s/n, E-08193 Barcelona, Spain*
[23]*Physik-Institut, University of Zürich, Winterthurerstrasse 190, CH-8057 Zürich, Switzerland*
[24]*Centro de Investigaciones Energéticas, Medioambientales y Tecnológicas (CIEMAT), Madrid, 28040, Spain*
[25]*Institute of Cosmology and Gravitation, University of Portsmouth, Portsmouth PO1 3FX, UK*
[26]*Department of Physics, Northeastern University, Boston, MA 02115, USA*
[27]*LMU Faculty of Physics, University Observatory, Scheinerstr. 1, D-81679 Munich, Germany*
[28]*Kavli Institute for Particle Astrophysics & Cosmology, Stanford University, PO Box 2450, Stanford, CA 94305, USA*

[29]*SLAC National Accelerator Laboratory, Menlo Park, CA 94025, USA*
[30]*Instituto de Astrofisica de Canarias, E-38205 La Laguna, Tenerife, Spain*
[31]*Laboratório Interinstitucional de e-Astronomia – LIneA, Av. Pastor Martin Luther King Jr, 126 Del Castilho, Nova América Offices, Torre 3000/sala 817 CEP: 20765-000, Brazil*
[32]*Institut de Física d'Altes Energies (IFAE), The Barcelona Institute of Science and Technology, Campus UAB, E-08193 Bellaterra (Barcelona), Spain*
[33]*Oxford College of Emory University, Oxford, GA 30054, USA*
[34]*Hamburger Sternwarte, Universität Hamburg, Gojenbergsweg 112, D-21029 Hamburg, Germany*
[35]*California Institute of Technology, 1200 East California Blvd, MC 249-17, Pasadena, CA 91125, USA*
[36]*Instituto de Fisica Teorica UAM/CSIC, Universidad Autonoma de Madrid, E-28049 Madrid, Spain*
[37]*Santa Cruz Institute for Particle Physics, Santa Cruz, CA 95064, USA*
[38]*Center for Cosmology and Astro-Particle Physics, The Ohio State University, Columbus, OH 43210, USA*
[39]*Department of Physics, The Ohio State University, Columbus, OH 43210, USA*
[40]*Department of Physics, University of Michigan, Ann Arbor, MI 48109, USA*
[41]*Center for Astrophysics | Harvard & Smithsonian, 60 Garden Street, Cambridge, MA 02138, USA*
[42]*Australian Astronomical Optics, Macquarie University, North Ryde, NSW 2113, Australia*
[43]*Lowell Observatory, 1400 Mars Hill Rd, Flagstaff, AZ 86001, USA*
[44]*Jet Propulsion Laboratory, California Institute of Technology, 4800 Oak Grove Dr, Pasadena, CA 91109, USA*
[45]*Centre for Gravitational Astrophysics, College of Science, The Australian National University, Canberra, ACT 2601, Australia*
[46]*George P. and Cynthia Woods Mitchell Institute for Fundamental Physics and Astronomy, and Department of Physics and Astronomy, Texas A&M University, College Station, TX 77843, USA*
[47]*Center for Astrophysical Surveys, National Center for Supercomputing Applications, 1205 West Clark St., Urbana, IL 61801, USA*
[48]*Department of Astronomy, University of Illinois at Urbana-Champaign, 1002 W. Green Street, Urbana, IL 61801, USA*
[49]*Institució Catalana de Recerca i Estudis Avançats, E-08010 Barcelona, Spain*
[50]*Institut de Física d'Altes Energies (IFAE), The Barcelona Institute of Science and Technology, Campus UAB, E-08193 Bellaterra (Barcelona), Spain*
[51]*Department of Physics, University of Cincinnati, Cincinnati, Ohio 45221, USA*
[52]*Perimeter Institute for Theoretical Physics, 31 Caroline St. North, Waterloo, ON N2L 2Y5, Canada*
[53]*Department of Astrophysical Sciences, Princeton University, Peyton Hall, Princeton, NJ 08544, USA*
[54]*Centro de Tecnologia da Informação Renato Archer, Campinas, SP-13069-901, Brazil*
[55]*Observatório Nacional, Rio de Janeiro, RJ-20921-400, Brazil*
[56]*Faculty of Physics and Astronomy, Astronomical Institute, German Centre for Cosmological Lensing, Ruhr University Bochum, D-44780 Bochum, Germany*
[57]*Nordita, KTH Royal Institute of Technology and Stockholm University, Hannes Alfvéns väg 12, SE-10691 Stockholm, Sweden*
[58]*School of Mathematics and Physics, University of Surrey, Guildford, Surrey, UK*
[59]*Department of Physics and Astronomy, Pevensey Building, University of Sussex, Brighton BN1 9QH, UK*
[60]*Computer Science and Mathematics Division, Oak Ridge National Laboratory, Oak Ridge, TN 37831, USA*
[61]*Cerro Tololo Inter-American Observatory, NSF's National Optical-Infrared Astronomy Research Laboratory, Casilla 603, La Serena, Chile*
[62]*Berkeley Center for Cosmological Physics, Department of Physics, University of California, Berkeley, CA 94720, USA*
[63]*US Lawrence Berkeley National Laboratory, 1 Cyclotron Road, Berkeley, CA 94720, USA*
[64]*INAF – Osservatorio Astronomico di Trieste, via G. B. Tiepolo 11, I-34143 Trieste, Italy*

This paper has been typeset from a TEX/LATEX file prepared by the author.